Preprints (www.preprints.org) | NOT PEER-REVIEWED | Posted: 4 July 2022 doi:10.20944/preprints202207.0027.v1

Article

Influence of Environmental Parameters and Fiber Orientation on Dissolution Kinetics of Glass Fibers in Polymer Composites

Andrey E. Krauklis [1,*], Hani Amir Aouissi [2,3,4], Selma Bencedira [5,6], Juris Burlakovs [7], Ivar Zekker [8], Irina Bute [1], and Maris Klavins [9]

[1] Institute for Mechanics of Materials, University of Latvia, Jelgavas Street 3, LV-1004 Riga, Latvia.
[2] Scientific and Technical Research Center on Arid Regions (CRSTRA), Biskra 07000, Algeria.
[3] Laboratoire de Recherche et d'Etude en Aménagement et Urbanisme (LREAU), USTHB, Algiers 16000, Algeria.
[4] Environmental Research Center (CRE), Badji-Mokhtar Annaba University, Annaba, 23000, Algeria.
[5] Laboratory of LGE, Department of Process Engineering, Faculty of Technology, UBMA, B. P12, Annaba 23000, Algeria.
[6] Environmental Research Center, BP. 2024, 23005, Sidi Amar, Annaba, Algeria.
[7] Chair of Rural Building and Water Management, Estonian University of Life Sciences, Kreutzwaldi 5, 51014 Tartu, Estonia.
[8] Institute of Chemistry, University of Tartu, 14a Ravila St., 50411 Tartu, Estonia.
[9] Department of Environmental Science, University of Latvia, Riga, Jelgavas Street 1, LV-1004, Latvia.
* Correspondence: andykrauklis@gmail.com; andrejs.krauklis@lu.lv; Tel.: +371-268-10-288.

Abstract: Glass fibers slowly dissolve and age when exposed to water molecules. Such a phenomenon also occurs when glass fibers are inside fiber-reinforced composites protected by the matrix. This environmental aging results in the deterioration of the mechanical properties of the composite. In structural applications, GFRPs are continuously exposed to water environments for decades (typically design lifetime is around 25 years or even more). During their lifetime, these materials are affected by various temperatures, pH acidity levels, mechanical loads, and the synergy of these factors. The rate of the degradation process depends on the nature of glass, sizing, fiber orientation, and environmental factors such as acidity, temperature, and mechanical stress. In this work, degradation of typical industrial grade R-glass fibers, when inside an epoxy fiber-reinforced composite, is studied experimentally and computationally. A Dissolving Cylinder Zero-Order Kinetic (DCZOK) model was applied and could describe the long-term dissolution of glass composites, considering the influence of fiber orientation (hoop vs transverse), pH (1.7, 4.0, 5.7, 7.0, and 10.0), and temperature (20, 40, 60, and 80 °C). The limitations of the DCZOK model and effects of sizing protection, accumulation of degradation products inside the composite, and water availability were discussed. Experimentally dissolution was measured using ICP-MS. Like for the fibers, for GFRPs also, the temperature showed an Arrhenius-type influence on the kinetics, increasing the rate of dissolution exponentially with increasing temperature. Similar to fibers, GFRPs showed a hyperbolic dependence on pH. The model was able to capture all of these effects, and the limitations were addressed.

Keywords: glass fibers; composites; environmental aging; modeling; kinetics; water; pH; temperature; orientation; durability

1. Introduction

The most commonly used type of fiber reinforcement is Glass Fiber (GF) [1-3]. GFs are hydrophilic and are susceptible to degradation; they dissolve due to environmental aging when exposed to water molecules when submerged in liquid media or humid environments [4]. The fact that GFs degrade in aqueous environments has been known at least since the early 1970s [5-7]. However, not all GFs degrade at the same rates [8]. Furthermore, this process, albeit slower, also occurs when GFs are encapsulated in composites – glass fiber-reinforced polymers (GFRPs) [9]. The encapsulated GFs are protected

© 2022 by the author(s). Distributed under a Creative Commons CC BY license.

Preprints (www.preprints.org) | NOT PEER-REVIEWED | Posted: 4 July 2022 doi:10.20944/preprints202207.0027.v1

by the sizing and surrounding polymer matrix [10]. Dissolution rates are lower for protected fibers in GFRPs than for single fibers or fiber bundles. However, this protection is insufficient to stop the degradation process altogether [10]. Such environmental aging results in the deterioration of the composites' mechanical properties, negatively affecting the strength and modulus of the GFRPs [11]. The negative effect can be so strong that it cannot be neglected when designing structural GFRPs for underwater and humid-environment use [12].

A typical design lifetime of GFRP structures in structural applications can range from 25 to 40 years or even more [13,14]. During this period, the GFRPs may be continuously exposed to water molecules, involving environmental degradation of the reinforcing GFs [12-14].

Glass formulation. The rate of the degradation process depends on the nature of glass material formulation (E, ECR, A, R, S-glass, etc.), sizing formulation, fiber orientation, and environmental factors such as acidity (pH), temperature, and mechanical stress [15,16]. The degradation rate may vary from extremely slow to extremely fast, based on material properties and environment, i.e., type of acid and pH. According to [17], degradation of GFRPs due to the environment's pH mostly depends on the type of glass fibers used. For example, boron-free glass fibers of ECR-type are considered the most inert, whereas our tests on R-glass have shown that R-glass fibers degrade relatively fast in strongly acidic environments. The GFRP pipes with ECR glass fibers are often used in strongly acidic applications, where they can withstand degradation for decades. ECR stands for E-glass Corrosion Resistant. It should not be confused with a most common E-glass, which degrades rather quickly when exposed to strong acid like the R-glass.

It was found that the corrosion resistance of the glass fibers varies enormously among the glass fiber types. Furthermore, the results indicate that the laminates' stress-corrosion properties correlate with the fibers' uniform corrosion resistance. The performance and reliability of an FRP structure exposed to aggressive environments can be strongly improved by choosing a corrosion-resistant fiber. The risk of stress-corrosion cracking can be reduced to a minimum level [18].

In this work, the degradation process of the typical industrial grade R-glass fibers (R-GF), when inside an epoxy fiber-reinforced composite, is studied experimentally and computationally.

Glass fiber dissolution kinetics determination. Current recycling strategies have attempted to mitigate the environmental harm caused by the disposal of end-of-life composite materials, some of which are currently being employed on an industrial basis [1]. Understanding and managing the dissolving process of fiber glass composites necessitates research into reaction kinetics. There has been a well-described dissolution of silicate glass within alkali solutions and environment [19], whereas glass fiber dissolution mechanism and kinetics are less documented (see following chapters for more detail). There has been found a reaction rate constant for glass fiber dissolution in alkaline solution at 95 °C to be at 1.3×10^{-4} - 4.3×10^{-4} g/(m^2 s). The reaction order (n) is at 0.31–0.49 in alkaline solution, with the activation energy being 58–79 kJ/mol [20].

Various studies have been done on the application of dissolution and elemental measurements of glass fibers, casework glass, headlamps in automotive applications [21], as well as glass in forensic science [22] by the use of mass spectrometric, spectroscopic and radiochemical techniques [23]. E-glass fibers have been put into reaction with a corrosive medium, removed residues, and found changes in fiber dimensions using a scanning electron microscope (SEM) [20]. Among spectrometric and mass spectrometric methods, glass materials composition has been characterized by techniques such as laser ablation inductively coupled plasma mass spectrometry (LA-ICP-MS) [24] and ICP-MS (especially suitable for multi-elemental determination), such as in this study [10,16,21,25,26]. LA-ICP-MS has the advantage over ICP-MS due to no need for sample dilution prior to analysis for the first one, however, the technique is not available, therefore ICP-MS is used in this study. In [27], a technique for determining the dissolving rate constant of a borosilicate

Preprints (www.preprints.org) | NOT PEER-REVIEWED | Posted: 4 July 2022 doi:10.20944/preprints202207.0027.v1

glass fiber in the lung, as determined in vitro, from the oxide composition in weight percent is described. Some other methods used for glass elemental characterization include atomic x-ray fluorescence [22], atomic absorption spectroscopy [24,28], SEM [29] and neutron activation [30]. Composite measurements by thermogravimetric analysis (TGA) could define the moisture, fiber content, and polymer content in GFRPs. Micro-computed tomography (μCT) has been applied to determine voids in glass and the fiber bundles geometry in polymers relying on fiber-reinforced glass (GFR) materials [31]. Optical coherence tomography (OCT), as a nondestructive method, has been used for GFR materials determination [32], whereas X-ray-CT surpasses the former technique by displaying more clearer reinforcement structure [31].

Environmental factors and orientation effect. The kinetics of the aging process depends on environmental factors such as temperature, acidity levels, and mechanical loads [16]. Previous studies have investigated these environmental effects experimentally and computationally for the same R-GFs (fiber bundles, not encapsulated into composites) [16,27]. Furthermore, the aging process also depends on the layup and orientation of the reinforcement GFs [10]. It involves composite-specific response effects such as sizing (also for sized GFs [10]) and matrix protection, accumulation of degradation products inside the composite, and water availability [10]. These effects have been studied for R-glass GFRPs with the identical layups and orientation as in this work in [10], however only in neutral conditions and without an influence of temperature. Hence, in this work, the synergy is investigated, proceeding from findings on the fiber orientation effects studied in [10] and the environmental impact on the R-GF bundle aging studied in [16].

However, it should also be noted that polymer matrix protects the glass in composites and should slow down the dissolution. There have been no conclusive results on how much matrix slows down the dissolution, except for a rare study, where it was found that even for thin composite plates, dissolution slows down about two times when glass fibers are embedded in a polymer [10]. Also, it was found that fiber orientation affects the glass dissolution rate. Dissolution degradation of GFRPs with fibers in hoop direction was slower than for the plates with transverse fiber orientation [10].

The molecular mechanism of R-GF degradation. Glass fiber dissolution degradation occurs when silica glass material (GF) is in contact with water molecules. A respective hydrolysis reaction takes place and is shown in Figure 1, according to [33].

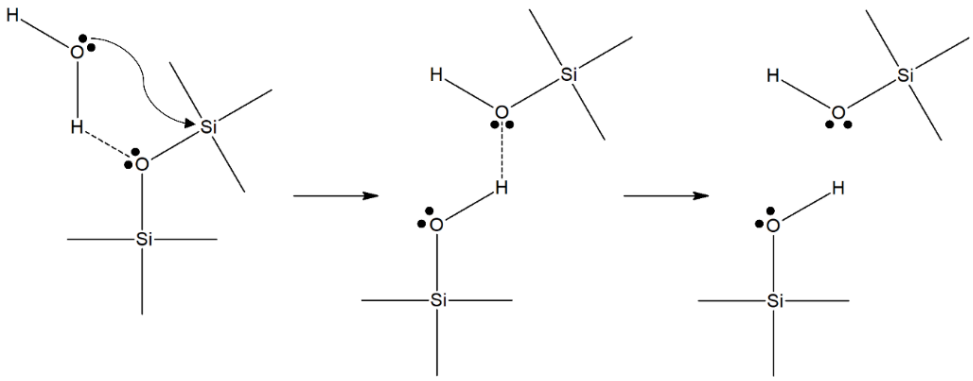

Figure 1. Hydrolysis chemical reaction of silica glass network, according to [33].

Most studies explain environmental degradation mechanisms of glass in terms of surface reactions, chemical affinity and diffusion [4,34-38]. However, dissolution experiments are mainly reported for bulk glass, whereas GFs and GFRPs are rarely studied [27]. However, some reflections on the mechanism of GF degradation do exist. The state-of-the-art mechanistic understanding of GF degradation is based on the works by Grambow

Preprints (www.preprints.org) | NOT PEER-REVIEWED | Posted: 4 July 2022 doi:10.20944/preprints202207.0027.v1

et al. (2001), Hunter *et al.* (2015) and Echtermeyer & Krauklis *et al.* (2018 & 2019) [11,16,27,39-40]. The complex nature of GF degradation involves several parallel processes, namely, gel layer formation, dissolution of glass matrix constituents, alkaline and alkaline earth ion exchange, and neoformation of solid reaction products. Some of these reactions occur in the glassy state, while others lead to the leaching of the reaction products into the surrounding aqueous environment [39,41]. Competing chemical reactions can be described by Equations (1)-(12), summarized after sources from 1979 up to 2022 [6,8,15,16,27,33,39-44]:

$$(\equiv \mathrm{Si-ONa}) + \mathrm{H_2O} \rightarrow (\equiv \mathrm{Si-OH}) + \mathrm{OH^-} + \mathrm{Na^+} \tag{1}$$

$$(\equiv \mathrm{Si-OK}) + \mathrm{H_2O} \rightarrow (\equiv \mathrm{Si-OH}) + \mathrm{OH^-} + \mathrm{K^+} \tag{2}$$

$$(\equiv \mathrm{Si-O})_2\mathrm{Ca} + \mathrm{H_2O} \rightarrow 2(\equiv \mathrm{Si-OH}) + 2\mathrm{OH^-} + \mathrm{Ca^{2+}} \tag{3}$$

$$(\equiv \mathrm{Si-O})_2\mathrm{Mg} + \mathrm{H_2O} \rightarrow 2(\equiv \mathrm{Si-OH}) + 2\mathrm{OH^-} + \mathrm{Mg^{2+}} \tag{4}$$

$$(\equiv \mathrm{Si-O-Al} =) + \mathrm{H_2O} \leftrightarrow (\equiv \mathrm{Si-OH}) + (= \mathrm{Al-OH}) \tag{5}$$

$$(\equiv \mathrm{Si-O})_2\mathrm{Fe} + \mathrm{H_2O} \rightarrow 2(\equiv \mathrm{Si-OH}) + 2\mathrm{OH^-} + \mathrm{Fe^{2+}} \tag{6}$$

$$(\equiv \mathrm{Si-O})_3\mathrm{Fe} + \mathrm{H_2O} \rightarrow 3(\equiv \mathrm{Si-OH}) + 3\mathrm{OH^-} + \mathrm{Fe^{3+}} \tag{7}$$

$$(\equiv \mathrm{Si-O-Si} \equiv) + \mathrm{OH^-} \leftrightarrow (\equiv \mathrm{Si-OH}) + (\equiv \mathrm{Si-O^-}) \tag{8}$$

$$(\equiv \mathrm{Si-O^-}) + \mathrm{H_2O} \leftrightarrow (\equiv \mathrm{Si-OH}) + \mathrm{OH^-} \tag{9}$$

$$\mathrm{SiO_2} + \mathrm{H_2O} \leftrightarrow \mathrm{H_2SiO_3} \tag{10}$$

$$\mathrm{H_2SiO_3} + \mathrm{H_2O} \leftrightarrow \mathrm{H_4SiO_4} \tag{11}$$

$$\mathrm{MeCl_x} \xrightarrow{\mathrm{H_2O}} (\mathrm{Me^{x+}}) + \mathrm{xCl^-} \tag{12}$$

The degradation of GFs proceeds in two phases. In the short-term non-steady-state (Phase I), hydrolytic degradation involves such competing processes (ion exchange, gel formation and dissolution). In the long-term steady-state (Phase II), hydrolytic degradation is governed by the glass dissolution mechanism and follows zero-order reaction kinetics [9,10,27]. Such kinetics depend on the glass surface area in contact with water, proportional to the fiber radius. As the dissolution continues, the radius decreases, resulting in the mass loss deceleration [9]. For the studied R-glass, the transition from Phase I into Phase II occurs in about a week (166 h) at pH 5.7 and 60 °C [9,10,27]. Elements that are released during degradation of R-glass are Na, K, Ca, Mg, Fe, Al, Si and Cl [27]. The experimental glass mass loss (measured by ICP-MS) is the cumulative mass loss of all these ions [27]. Si contribution to the total mass loss of the studied R-glass is the largest (56.1 wt%) and seems to govern the dissolution process [27].

The dissolution-driven degradation is an energy-activated process. It is known, that for non-embedded R-GFs, the process follows the Arrhenius principle well – the rate of dissolution increases as the temperature increases [16]. The temperature dependence of a dissolution rate constant can be described using the Arrhenius equation (Equation 13), being an exponential function:

$$K_0 = Ae^{-\frac{E_A(pH,\sigma)}{RT}} \tag{13}$$

where A is the pre-exponential factor (g/(m²·s)); R is the gas constant being 8.314 J/(mol·K); T is the absolute temperature (K); E_A is the activation energy (J/mol). Both pH

Preprints (www.preprints.org) | NOT PEER-REVIEWED | Posted: 4 July 2022 doi:10.20944/preprints202207.0027.v1

and stress corrosion affect the activation energy term in the Arrhenius equation [16]. Mechanical stress accelerates the rate due to a stress-corrosion mechanism [16]. However, the most prominent environmental influence on the kinetics is due to the parabolic pH influence. The dissolution rate is slowest at conditions close to neutral and accelerates towards both acidic and basic ends, especially in highly acidic environments [16].

In this work, dissolution kinetics was measured experimentally using ICP-MS. A Dissolving Cylinder Zero-Order Kinetic (DCZOK) model was then applied to investigate the long-term dissolution of glass composites computationally, considering the influence of fiber orientation, pH, and temperature. This model was chosen for the calculations because it considers the complex short-term and dissolution-dominated long-term processes, describes dissolution and is able to link it with radius reduction kinetics, crack-growth kinetics, and strength drop kinetics [11]. Another aspect of the choice of calculation model was ability to avoid introducing additional terms such as conversion factor [27]. The DCZOK model is described in more detail in [16,27], similarly as was done in two studies mentioned above involving neutral environment effect on GFRPs [10] and environmental effects on R-GF [16]. The total material loss and release of Si under various environmental conditions were simulated using the DCZOK model, and rate constants were obtained and reported.

The benefit for the industry. The industry is interested in pH, temperature, and stress corrosion for environmental effects [16]. Temperatures are also attractive to the industry for accelerated testing purposes [12]. As the industry is concerned with lowering the testing time for fiber-dominated property deterioration in GFRPs, the model considerably shortens experimental testing time to short-term and slightly into the long-term steady-state to obtain model parameters, i.e., kinetic constants and time to reach steady-state. While it takes time to obtain the parameters, the most significant time saving comes from using the kinetic constants and the model [12,15,45].

Along with the current technological limitations of composite recycling (although the technology is rapidly developing) [1], the environmental durability of GFRPs stays one of the limiting factors to the development of the composite industry [12,46]. This is due to the superior mechanical properties being compromised by the uncertainty of the material's interaction with the environment [47]. Modeling can lighten these questions and solve the problem at hand [12].

In the state-of-the-art, an analytical modelling toolbox (Modular Paradigm for GFRPs) consisting of seven modules for reinforcement materials was described in [8]. The work [8] states that extension of DCZOK model to GFRPs is currently a major challenge. Therefore, this study contributes to a better understanding of modelling mass loss of glass fibers in GFRPs (Module 4 in [8]).

This study aims to experimentally characterize the environmental aging of R-GFRPs in various fiber orientations and environmental conditions and to capture this behavior computationally using the DCZOK model. The secondary aim is to investigate the limitations of the DCZOK model and better understand the effects of sizing protection, accumulation of degradation products inside the composite, and water availability.

2. Materials and Methods

2.1. Materials

Glass Fibers. Common industrial-grade boron-free and fluorine-free 3B HiPer-Tex W2020 R-GF was studied as a reinforcement material (in the form of stitch-bonded fabrics). 3B HiPer-Tex W2020 R-glass is classified as a high-strength and high modulus R-glass per definition by an international standard [48]. The average fiber diameter was 17 ± 2 μm, and density was 2.54 g/cm^3, as reported in the previous experimental and modeling studies on the same material [16,49]. The authors have estimated 4098 fibers per bundle in a mat on average [16,49]. The specific surface area was 0.09 m^2/g from geometrical considerations (as a product of the number, circumference, and length of the fibers [27])

Preprints (www.preprints.org) | NOT PEER-REVIEWED | Posted: 4 July 2022 doi:10.20944/preprints202207.0027.v1

and 0.18 m^2/g according to Brunaer-Emmett-Teller (BET) tests, the difference explained by uneven sizing distribution [26]. All reinforcement within this study had the same sizing W2020 (typical industrial epoxy-compatible sizing) as in the previous studies [9-11,16,26,27].

The dissolution of the same unsized R-glass fibers was previously studied in other works by Krauklis and Echtermeyer [9-11,16,26,27]. Also, GFRPs with the same fibers and sizing but limited environmental conditions were studied in [10]. This work is a continuation of these studies and an investigation of synergy.

Polymer Composites. Composites were prepared using vacuum-assisted resin transfer molding (VARTM) process in two unidirectional configurations (fiber orientations): in-plane (hoop orientation when cut from a pipe) and out-of-plane (transverse direction when cut from a pipe) – see Figure 2 for a clear visual.

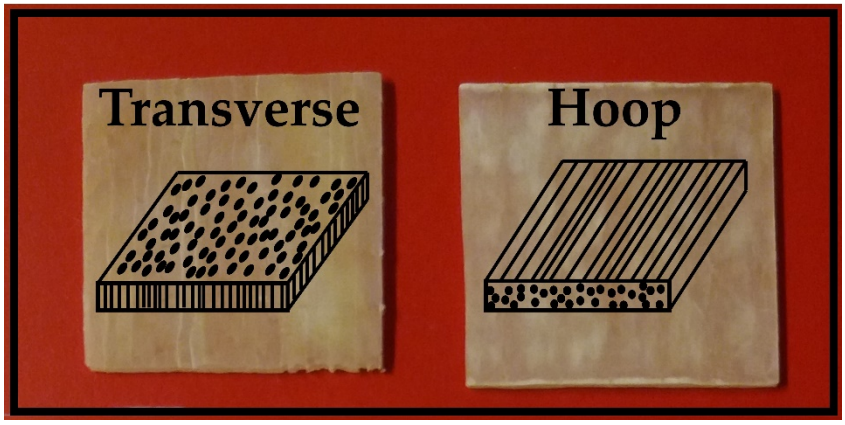

Figure 2. GFRP plate specimen fiber orientations: (left) transverse and (right) hoop orientations.

Composite laminates were prepared via Vacuum-Assisted Resin Transfer Molding (VARTM) using Hexion epoxy resin RIMR135 and amine hardener RIMH137 in the stoichiometric proportion of 100:30 (weight ratio). The resin and the curing agent consisted of bisphenol A diglycidyl ether (DGEBA), 1,6-hexanediol diglycidyl ether (HDDGE), poly(oxypropylene) diamine (POPA), and isophorondiamine (IPDA). Before VARTM, the epoxy/hardener mixture was degassed in a vacuum chamber for 30 min to remove bubbles. Curing was performed at room temperature for 24 h, followed by post-curing in an air oven at 80 °C for 16 h. The composite laminate was cut into rectangular bars and subsequently into composite plates with dimensions 20 x 20 x 1.5 mm with fibers oriented parallel (hoop-orientation plates) and normal (transverse-orientation plates) to the large face of the plate, respectively (as shown in Figure 2). The specified dimensions were achieved within 5 percent tolerance.

The specimens were dried for two weeks after the preparation procedures until the equilibrium. Water content was monitored via gravimetric method and a Fourier transform infrared (FTIR) spectroscopy composite water monitoring method, described in [50]. FTIR spectra were recorded using Varian Scimitar 800 FT-IR in the Attenuated Total Reflectance (ATR) mode via Pike technologies GladiATR™ mode. Spectra were obtained at 4 cm^{-1} resolution, co-adding 50 scans over a range of wavenumbers from 400 to 4000 cm^{-1}.

GFRP plate specimen configurations are summarized in the Table 1.

Table 1. GFRP plate specimen configurations.

Geometry [mm]	20 x 20 x 1.5
Loss On Ignition (LOI)	0.0064
Composite density [g/cm^3]	1.93
Glass density [g/cm^3]	2.54

Preprints (www.preprints.org) | NOT PEER-REVIEWED | Posted: 4 July 2022 doi:10.20944/preprints202207.0027.v1

Polymer density [g/cm³]	1.1
Sizing density [g/cm³]	1.1
Fiber volume fraction	0.5950
Void volume fraction	0.0044
Polymer volume fraction	0.3920
Sizing/interphase volume fraction	0.0087
Fiber mass fraction	0.7723
Polymer mass fraction	0.2227
Sizing/interphase mass fraction	0.0049

Aging medium. Distilled water (0.5-1.0 MΩ·cm) was used for conditioning the R-GFRP specimens. The pH of the distilled water was 5.65 ± 0.01, being lower than neutral due to dissolved CO_2 from the atmosphere in equilibrium. IUPAC standard buffer solutions (Radiometer analytical, France) were used to study pH's effect on the kinetics of R-GFRP dissolution. The solutions of pH 1.679, 4.005, 5.650, 7.000 and 10.012 were used. pH solutions were checked using the standard pH-meter MeterLab PHM210 with an accuracy of ± 0.01 pH. All specimens were put dry into the water solutions, meaning they were all saturated at their respective pH and temperature.

2.2. Methods

Glass fiber fraction determination. The fraction of the glass fibers of the GFRP composite specimens was determined by the burn-off test, after the ASTM Standard D3171, and used in density considerations [51]. The density of matrix polymer (ρ_{matrix}) and glass fiber (ρ_{glass}) was 1.1 g/cm³ and 2.54 g/cm³, respectively. The density of the composite (ρ_{GFRP}) was determined to be 1.93 g/cm³ by measuring the mass and dimensions of a large GFRP composite block. The volume and mass fractions of matrix polymer can then be calculated using Equations 14 and 15, respectively.

$$V_f = \frac{\rho_{GFRP} - \rho_{matrix}}{\rho_{glass} - \rho_{matrix}} \tag{14}$$

$$m_f = \frac{\rho_{glass} \cdot V_f}{\rho_{matrix} \cdot (1 - V_f) + \rho_{glass} \cdot V_f} \tag{15}$$

The volume and mass fraction of fibers was V_f = 0.595 and m_f = 0.772, respectively. The void content was very low (0.44%), similar to [52].

Diffusion measurements and environmental aging. Dissolution experiments in the water of GFRP specimens were conducted using a batch system. Specimens for the dissolution study were weighed using analytical scales AG204 (with precision of ± 0.1 mg) before and during the experiments. The specimens were placed in inert closed vessels filled with 50 mL of distilled water or pH buffer solutions. The tight sealing of specimens was ensured. The water-tight containers, with specimens and water solutions in them, were placed in the water bath. The gravimetric water uptake was measured for GFRP plates in hoop and transverse orientations at pH 5.65 at 60 °C to ensure that the saturation with water was reached. The bath's water temperature (20, 40, 60, and 80 °C) was controlled via PID-controlled heating, giving an accuracy of ± 1 °C. The two-stage heating system was used to ensure that there is no contact of the sample water with other potential ion release sources, such as the heating element itself.

Microscopy of aged specimens. Optical microscopy was performed using a digital microscope Hirox RH-2000 equipped with lens MXB-2500REZ with a magnification of 140 and resolution of 1.06 µm. Microscopy was used for inspecting changes in GFRP structure and morphology after various environmental aging conditions.

Preprints (www.preprints.org) | NOT PEER-REVIEWED | Posted: 4 July 2022 doi:10.20944/preprints202207.0027.v1

Glass material dissolution (ion release) measurements. The concentration of dissolved ions was analyzed in time via inductively coupled plasma mass spectrometry (ICP-MS), providing glass material dissolution kinetics experimentally. A total mass loss of glass material was measured as a sum of all ions' release quantified with ICP-MS (cumulatively over time). Analyses were performed using a double-focusing magnetic sector field ICP-MS Finnigan ELEMENT 2 (Thermo-Scientific), equipped with a sample introduction system PrepFAST (ESI/Elemental Scientific) and a pre-treatment/digestion UltraClave (Milestone). Acidification of samples was performed using ultra-pure grade HNO_3 SubPur (Milestone) to avoid adsorption of ions to the wall of the sample vials. Experiments were performed with three parallels.

The benefit of ICP-MS versus gravimetric analysis is that it allows for measuring the dissolution kinetics of each separate ion, as well as the total mass loss [27]. In addition, it allows to decouple inorganic material degradation, such as glass, from the organic polymer. The data obtained from the ICP-MS experiments are in the form of mass concentration at each time point (non-cumulative) c (g/L) and are converted to the $m_{dissolved}$ form by using Equation 16:

$$m_{dissolved} = V_{water} \int_0^t c\, dt \tag{16}$$

where V_{water} is the volume of a water sample in the ICP-MS measurement. V_{water} used for experiments was 50 mL. Equation 3 is valid for each ion release and the total mass loss.

The Dissolving Cylinder Zero-Order Kinetics (DCZOK) Model. The analytical DCZOK model can predict the mass loss kinetics, fiber radius reduction kinetics, hydrolytic flaw growth kinetics, as well as hydrolysis-induced strength degradation kinetics of unembedded R-GFs [9,11]. The dissolution of GFs inside composites is slowed down compared to GF bundles and is addressed in the analytical model [10].

For fibers, in infinite water availability conditions, the dissolution, which is a surface reaction, can be well-described with zero-order kinetics [27]. Still, the decrease in fiber radius and thus a decrease in surface area with time should be accounted for [27]. For sized fibers, the effect of sizing ξ_{sizing} should also be accounted for [10]. The effect of sizing on glass dissolution ξ_{sizing} for the studied R-glass is 0.165, protecting fibers from water by almost an order of magnitude in terms of dissolution rates [10]. For sized fiber bundles (not embedded in the composite), the mass loss kinetic model equation in differential form is (Equation 17):

$$\frac{\partial m}{\partial t} = 2n\pi l \left(r_0 K_0 \xi_{sizing} - \frac{K_0^2 \xi_{sizing}^2}{\rho_{glass}} t \right) \tag{17}$$

The radius reduction over time is accounted for in the model; the environmental parameters and their synergy, such as, pH, temperature, and stress corrosion affect the material-environment energy-activated interactions, thus affecting the dissolution rate constants K_0 [9]. For unembedded R-GFs, the DCZOK model was successfully applied to account for the environmental conditions (pH, T, σ), Equation 18 [16]:

$$\frac{\partial m}{\partial t} = 2n\pi l \left(r_0 A e^{-\frac{E_A(pH,\sigma)}{RT}} \xi_{sizing} - \frac{\left(A e^{-\frac{E_A(pH,\sigma)}{RT}} \xi_{sizing} \right)^2}{\rho_{glass}} t \right) \tag{18}$$

where m is a total cumulative mass dissolved after time t; K_0 is a material/environment interaction property; ξ_{sizing} is the protective effect of sizing; pH is the acidity of the environment (-), T is its temperature (K); σ is mechanical stress (MPa); n is the number of

Preprints (www.preprints.org) | NOT PEER-REVIEWED | Posted: 4 July 2022 doi:10.20944/preprints202207.0027.v1

fibers (-); l is the length of fibers (m); r_0 is the initial fiber radius (m); ρ_{glass} is the density of glass (g/m³); A is the pre-exponential factor (g/(m²·s)); R is the gas constant being 8.314 J/(mol·K); T is the absolute temperature (K); E_A is the activation energy (J/mol).

For GFRPs, an extended case of the DCZOK model is required, discussed in [9,10]. As the ageing advances, the degradation products are accumulated inside the composite material and subsequently slow down the reaction rate of glass fiber dissolution by shifting the chemical equilibrium. Since the long-term response is governed by Si dissolution [27], the silica hydrolysis products cause the deceleration of glass dissolution inside the composites [9]. In the model, the accumulation term accounts for a "driving force" term, which shows that the mass-loss rate is proportional to the difference between concentrations of degradation products inside the composite at saturation and at a specific time point [10]. The extended DCZOK model can be mathematically expressed as Equations 19 and 20, and considering environmental effects described by Equation 13 [9,10,16]:

$$\frac{\partial m}{\partial t} = K_0 \xi_{sizing} S C_{H_2O}^{n_{order}} \left(C_{SiO_2}^{eq} - C_{SiO_2}\right)^{m_{order}} \cong K_0^* S \tag{19}$$

$$\frac{\partial m}{\partial t} = 2n\pi l \left(r_0 K_0 \xi_{sizing} C_{H_2O}^{n_{order}}(t) \left(\frac{C_{SiO_2}^{eq} - C_{SiO_2}(t)}{C_{SiO_2}^{eq}} \right)^{m_{order}} - \frac{\left(K_0 \xi_{sizing} C_{H_2O}^{n_{order}}(t) \left(\frac{C_{SiO_2}^{eq} - C_{SiO_2}(t)}{C_{SiO_2}^{eq}} \right)^{m_{order}} \right)^2}{\rho_{glass}} t \right) \tag{20}$$

$$K_0 = A e^{-\frac{E_A(pH,\sigma)}{RT}} \tag{13}$$

where m is a total cumulative mass dissolved after time t; K_0^* is an apparent reaction kinetic constant that can be obtained from regression of experimental data. While K_0 is a material property, K_0^* incorporates effects of sizing, water availability and degradation product accumulation; n is the number of fibers (-); l is the length of fibers (m); r_0 is the initial fiber radius (m), and ρ_{glass} is the density of glass (g/m³); ξ_{sizing} is the protective effect of the sizing; S is the glass surface area exposed to water; C_{H_2O} is the availability of water molecules to the reacting glass surface; n_{order} is the order of the reaction; $C_{SiO_2}^{eq}$ is the concentration of degradation products at saturation inside the composite; C_{SiO_2} is the current concentration of degradation products inside the composite; and m_{order} is the order of the driving force term.

Assumptions. The model involves the following assumptions. As a simplification, this model is deterministic and all fibers are assumed to have the same initial radius r_0; the cross-sectional surface area at the end of the fibers is assumed to be negligible in calculations of the surface area; the length of the long fibers l is assumed to be constant during the whole dissolution process. During the whole degradation process, the density of the glass material is assumed constant ρ_{glass}. The effect of sizing ξ_{sizing} is assumed to be independent of environmental conditions and time [9,10]. For the studied R-GFRPs, the protective effect of sizing ξ_{sizing} (0.165) on glass fiber dissolution was found to be about six times [10]. For free fiber bundles (not embedded in the composite) the conditions of infinite availability of water are ensured by using large volumes of water, thus making the rate of reaction independent of the water concentration [10]. For composites, as the aging proceeds, degradation products are accumulated inside the composite plates and slow down the rate of the reaction. Since the long-term reaction is governed by Si dissolution [27], the silica hydrolysis products are what causes the deceleration of glass dissolution inside the composites. In the model, the accumulation term is accounted for as a driving force term, that shows that rate of the mass loss is proportional to the difference

Preprints (www.preprints.org) | NOT PEER-REVIEWED | Posted: 4 July 2022 doi:10.20944/preprints202207.0027.v1

between saturation ($C_{SiO_2}^{eq}$) and current concentration (C_{SiO_2}) of degradation products in the composite and the order (m_{order}). The order of the water availability n_{order} accounts for the effect in which state the water is present in the polymer surrounding the glass, i.e., in a free, bound, or mixed state; thus, if eclectic, it can be a fractional number. The closer n_{order} is to 0, the more water is in the free state. For free fiber bundles (not embedded in the composite) in a large volume of water, conditions of infinite availability of water ensue, the rate of reaction becomes independent of the water concentration, and the water availability order n_{order} becomes 0 [9,10].

3. Results

Microscopy. The authors have performed a short experimental study earlier by immersing thin R-glass/epoxy GFRP plates (with two fiber orientations, hoop and transverse, respectively) at various pH to see whether there was significant damage due to short-term hydrolysis of glass fibers in GFRPs. GFRPs were immersed in aqueous solutions of pH 1.7, 4.0, 5.65, 7.0, and 10.0. The results are shown in Figure 3.

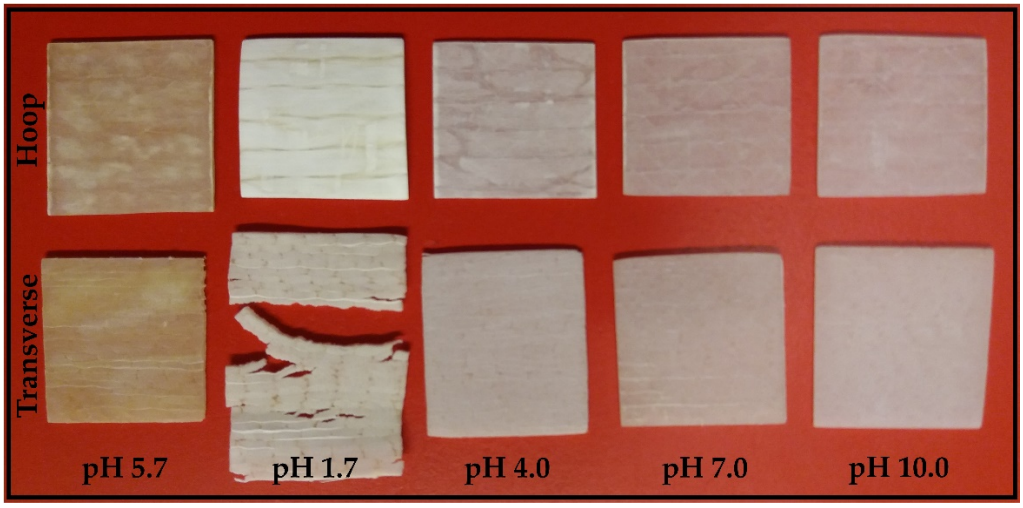

Figure 3. Effect of various pH aqueous solutions on the degradation of R-glass GFRP plates with two fiber orientations (hoop and transverse-orientation) after about a week (pH 1.7, 4.0, 7.0 and 10.0) and after four months (pH 5.7) of exposure.

Composite plates with two fiber orientations (hoop and transverse) are shown in Figure 3 and microscopy images in Figures 4-11. GFRP plates were exposed to aqueous solutions of various pH for a few days at room temperature. The composite specimens quickly degrade at pH 1.7 and are destroyed within a week, as seen in Figure 3. Thus, GFRPs should not be used in strongly acidic conditions. This observation is in full accord with a finding in another study, stating that many GFRPs fail catastrophically after a critical time when exposed to acids [17]. Furthermore, it can be seen that failure occurred on the surface of fibers, meaning that it was either due to the failure of glass fibers or the fiber-matrix interphase, which agrees with [26].

Even though the studied R-glass was boron-free (without any additional boron introduced during manufacturing, as indicated by the datasheets), it still degraded rapidly at pH 1.7 (Figures 3 and 4). For more acidic applications, the use of ECR-glass fiber reinforced composites should be considered and evaluated, as it is likely more suited than the R-glass composites [17], but experimental trials must be performed to verify this.

Preprints (www.preprints.org) | NOT PEER-REVIEWED | Posted: 4 July 2022 doi:10.20944/preprints202207.0027.v1

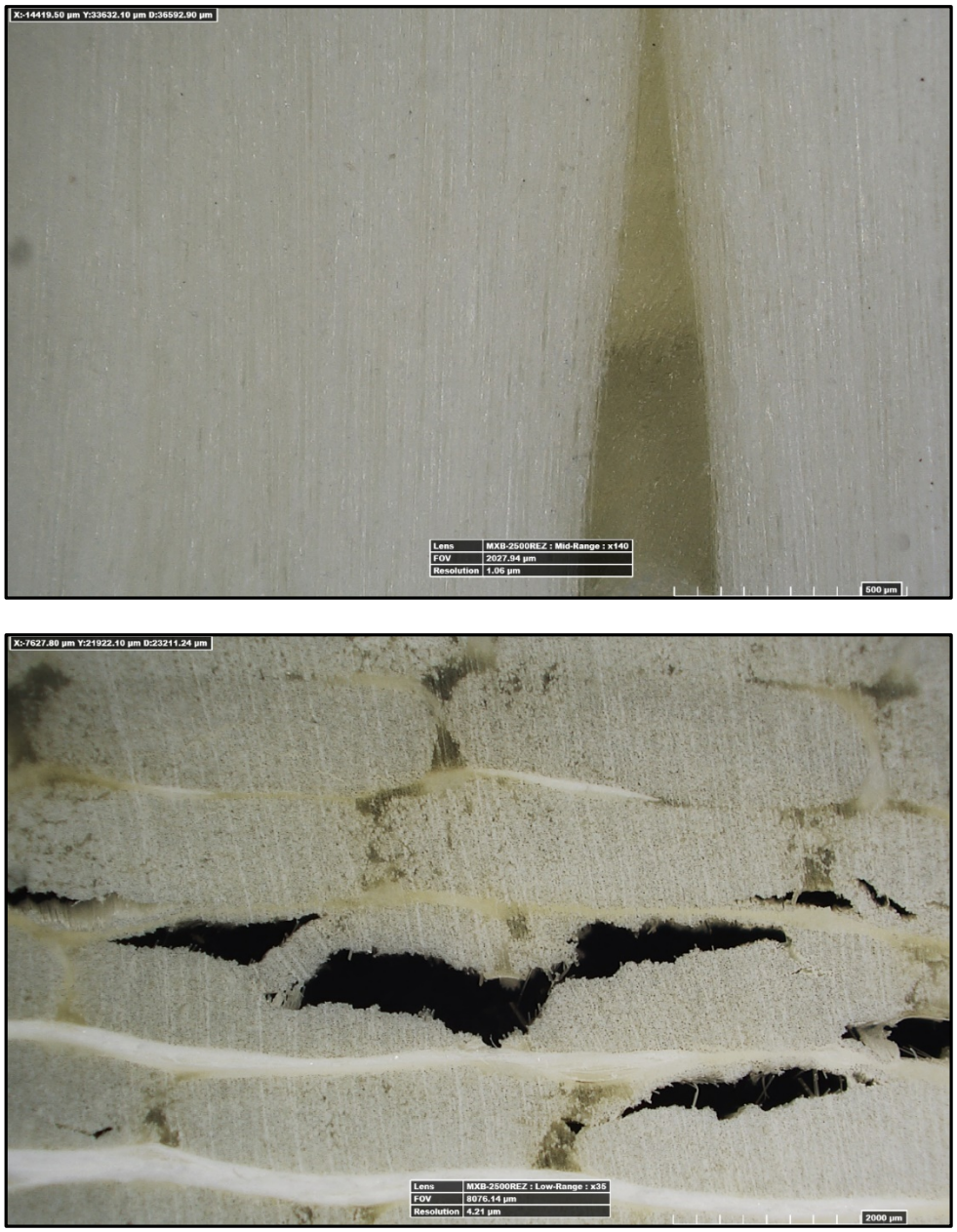

Figure 4. R-glass FRP plate with a (bottom) transverse and (top) hoop fiber orientation transverse-orientation after a week of exposure to pH 1.7 aqueous solution.

Preprints (www.preprints.org) | NOT PEER-REVIEWED | Posted: 4 July 2022 doi:10.20944/preprints202207.0027.v1

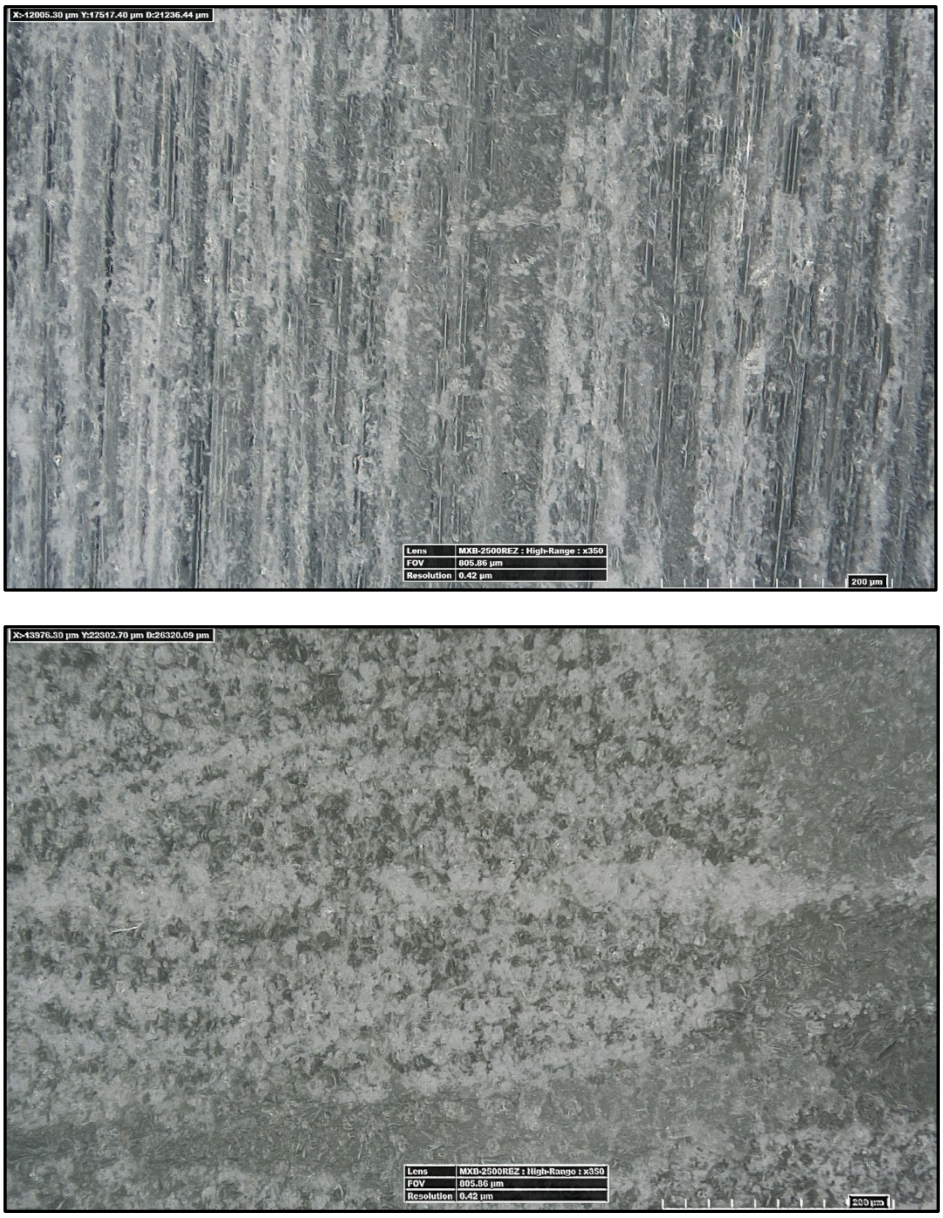

Figure 5. R-glass FRP plate with a (bottom) transverse and (top) hoop fiber orientation transverse-orientation after a week of exposure to pH 4.0 aqueous solution.

Preprints (www.preprints.org) | NOT PEER-REVIEWED | Posted: 4 July 2022 doi:10.20944/preprints202207.0027.v1

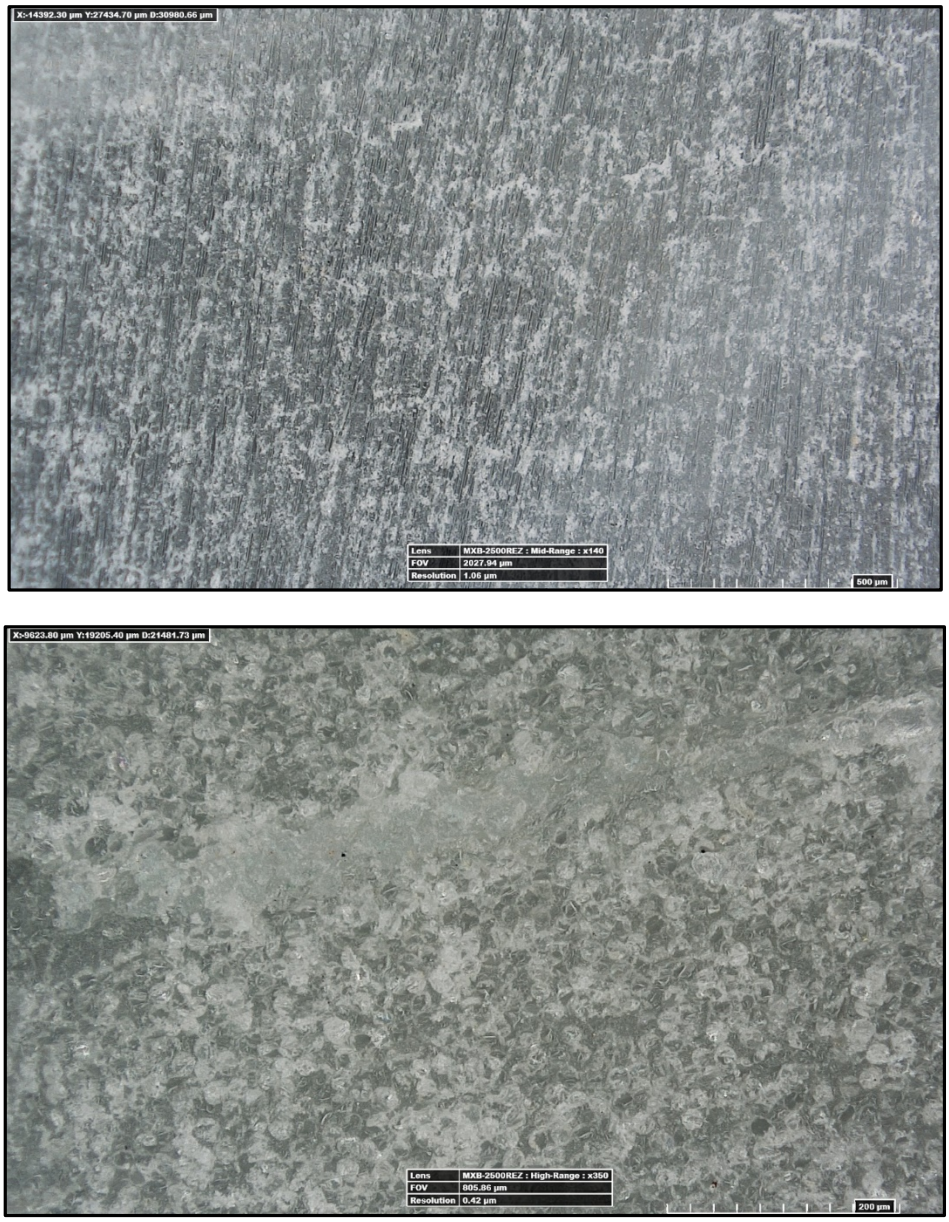

Figure 6. R-glass FRP plate with a (bottom) transverse and (top) hoop fiber orientation transverse-orientation after a week of exposure to pH 7.0 aqueous solution.

Preprints (www.preprints.org) | NOT PEER-REVIEWED | Posted: 4 July 2022 doi:10.20944/preprints202207.0027.v1

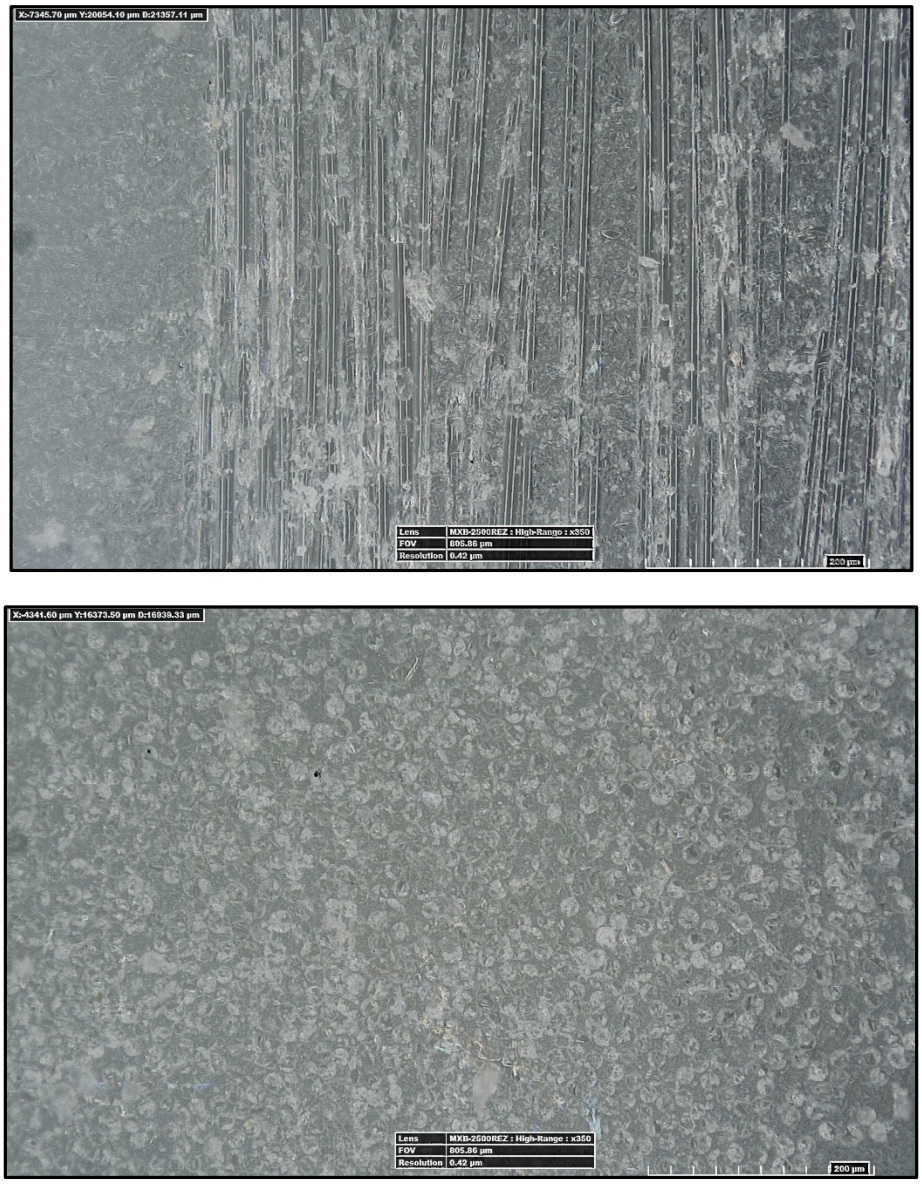

Figure 7. R-glass FRP plate with a (bottom) transverse and (top) hoop fiber orientation transverse-orientation after a week of exposure to pH 10.0 aqueous solution.

Diffusion measurements. The experimental gravimetric measurements for composite plates were performed to ensure that the R-GFRPs were saturated with water during the steady-state ion release kinetics measurements; the experimetnal weight gain curves are reported in Figure 8 for 4 months or 3000 h (54.7 $h^{0.5}$), along the simulated Fickian diffusion.

Preprints (www.preprints.org) | NOT PEER-REVIEWED | Posted: 4 July 2022 doi:10.20944/preprints202207.0027.v1

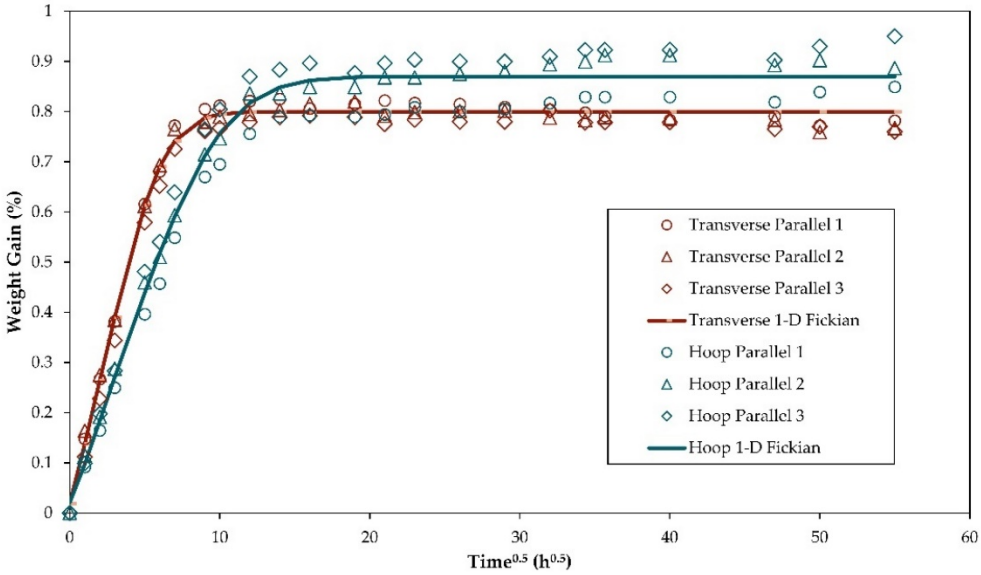

Figure 8. Water diffusion measurements.

The modeling curves shown in Figure 8 were obtained using 1-D analytical solutions to Fick's 2nd law applied for anisotropic materials from Crank [53], and more specifically for plate case, as reported in [54]. Relations for calculating water contents $w(t)$ are obtained by integration over the sample volume; these could be found elsewhere for orthotropic composite plates [54].

The equilibrium water uptake coeffiecients were 0.87 ± 0.08 wt% and 0.80 ± 0.05 wt% for hoop and transverse specimens, respectively. The water uptake was faster for composite plates with fibers in transverse orientation than for hoop orientation. This is in accord with literature on water diffusion in plates [54,55]. The diffusivites were 0.0038 ± 0.0008 mm²/h and 0.0108 ± 0.0005 mm²/h for hoop and transverse specimens, respectively. The goodness-of-fit for hoop and transverse was 0.9970 and 0.9993 (determined by R^2).

There is a long-term mass gain and mass loss observed for hoop and tranverse specimens, respectively, which is in accord with previous findings on the hydrolytic flaw formation mechanism in the composite interphase, described in detail in [26].

Ion release measurements. Ion release was measured for 4 months (3000 h) as well. From the measured concentration cumulative data of released ions during the dissolution of glass, the dissolution rate constants were obtained using non-linear regression for Si ($K^{I}_{0_{Si}}$ and $K^{II}_{0_{Si}}$) and for the total mass loss ($K^{I}_{0_{total}}$and $K^{II}_{0_{total}}$). The Generalized Reduced Gradient (GRG) non-linear regression method was used by minimizing the sum of squares of the differences between modeled and experimental values. The obtained parameters are systematized in Tables 2 and 3 for the impact of pH and temperature on dissolution kinetics, respectively. Obtained values are reasonable (similar order of magnitude) compared with dissolution rates of other glass fibers studied in the literature [16]. The dissolution rate constants for glass dissolution from GFRPs in water at various pH at 60 ± 1 °C are shown in Table 2. The steady-state was achieved after about a week (about the same time as saturation with water).

Table 2. The glass dissolution rate constants were obtained via regression of the experimental data of GFRPs using the DCZOK model for Si and total mass loss at 60 °C and various pH for both Hoop and Transverse orientations.

pH	$K^{I}_{0_{Si}}$ (g/(m²·s))	$K^{II}_{0_{Si}}$ (g/(m²·s))	$K^{I}_{0_{total}}$(g/(m²·s))	$K^{II}_{0_{total}}$(g/(m²·s))	*Reference*
R-GF					
1.679 ± 0.010	(3.10±0.44)·10⁻⁷	(1.25±0.09)·10⁻⁷	(1.70±0.19)·10⁻⁶	(1.16±0.08)·10⁻⁶	[16]
4.005 ± 0.010	(2.59±0.33)·10⁻⁸	(1.70±0.11)·10⁻⁸	(8.48±1.21)·10⁻⁸	(6.24±0.36)·10⁻⁸	[16]

Preprints (www.preprints.org) | NOT PEER-REVIEWED | Posted: 4 July 2022 doi:10.20944/preprints202207.0027.v1

5.650 ± 0.010	(6.67±1.03)·10^{-9}	(2.30±0.16)·10^{-9}	(1.82±0.29)·10^{-8}	(4.05±0.29)·10^{-9}	[16]
7.000 ± 0.010	(3.64±0.53)·10^{-8}	(2.55±0.19)·10^{-8}	(5.46±0.82)·10^{-8}	(4.85±0.38)·10^{-8}	[16]
10.012 ± 0.010	(8.97±1.27)·10^{-8}	(4.56±0.32)·10^{-8}	(1.39±0.16)·10^{-7}	(1.11±0.07)·10^{-7}	[16]
Hoop R-GFRP					
1.679 ± 0.010	(2.58±0.44)·10^{-8}	(1.80±0.12)·10^{-8}	(1.19±0.18)·10^{-7}	(1.10±0.08)·10^{-7}	This work
4.005 ± 0.010	(8.80±1.27)·10^{-10}	(8.12±0.69)·10^{-10}	(4.60±0.69)·10^{-9}	(3.50±0.32)·10^{-9}	This work
5.650 ± 0.010	(1.92±0.32)·10^{-10}	(1.32±0.10)·10^{-10}	(2.95±0.41)·10^{-9}	(5.35±0.42)·10^{-10}	This work
7.000 ± 0.010	(9.00±1.10)·10^{-10}	(8.20±0.53)·10^{-10}	(5.32±0.71)·10^{-9}	(4.28±0.28)·10^{-9}	This work
10.012 ± 0.010	(1.47±0.25)·10^{-8}	(7.44±0.71)·10^{-9}	(2.28±0.35)·10^{-8}	(1.78±0.11)·10^{-8}	This work
Transverse R-GFRP					
1.679 ± 0.010	(4.98±0.72)·10^{-8}	(2.03±0.12)·10^{-8}	(2.76±0.42)·10^{-7}	(1.91±0.13)·10^{-7}	This work
4.005 ± 0.010	(1.80±0.29)·10^{-9}	(1.70±0.11)·10^{-9}	(7.00±1.08)·10^{-9}	(6.00±0.47)·10^{-9}	This work
5.650 ± 0.010	(7.71±0.92)·10^{-10}	(2.40±0.19)·10^{-10}	(5.66±0.79)·10^{-9}	(5.87±0.41)·10^{-10}	This work
7.000 ± 0.010	(2.00±0.24)·10^{-9}	(1.90±0.12)·10^{-9}	(5.80±0.78)·10^{-9}	(4.80±0.35)·10^{-9}	This work
10.012 ± 0.010	(1.46±0.21)·10^{-8}	(7.51±0.53)·10^{-9}	(2.30±0.33)·10^{-8}	(1.82±0.14)·10^{-8}	This work

The dissolution rate constants for glass dissolution from GFRPs in water at various temperatures at pH 5.65 are shown in Table 3. The steady-state was achieved also after about a week.

Table 3. The glass dissolution rate constants were obtained via regression of the experimental data of GFRPs using the DCZOK model for Si and total mass loss at pH 5.65 and various temperatures for both Hoop and Transverse orientations.

T (°C)	$K^{I}_{0_{Si}}$ *(g/(m²·s))*	$K^{II}_{0_{Si}}$ *(g/(m²·s))*	$K^{I}_{0_{total}}$ *(g/(m²·s))*	$K^{II}_{0_{total}}$ *(g/(m²·s))*	*Reference*
R-GF					
20 ± 1	(1.46±0.23)·10^{-9}	(2.60±0.18)·10^{-10}	(1.04±0.12)·10^{-8}	(1.42±0.11)·10^{-9}	[16]
40 ± 1	(2.62±0.37)·10^{-9}	(1.08±0.08)·10^{-9}	(1.37±0.19)·10^{-8}	(2.72±0.19)·10^{-9}	[16]
60 ± 1	(6.67±1.03)·10^{-9}	(2.30±0.16)·10^{-9}	(1.82±0.29)·10^{-8}	(4.05±0.29)·10^{-9}	[16]
80 ± 1	(2.19±0.31)·10^{-8}	(8.91±0.73)·10^{-9}	(4.24±0.59)·10^{-8}	(1.47±0.11)·10^{-8}	[16]
Hoop R-GFRP					
20 ± 1	(6.96±0.97)·10^{-11}	(3.64±0.28)·10^{-11}	(9.02±0.12)·10^{-10}	(2.05±0.16)·10^{-10}	This work
40 ± 1	(1.71±0.22)·10^{-10}	(8.02±0.58)·10^{-11}	(1.78±0.27)·10^{-9}	(3.49±0.23)·10^{-10}	This work
60 ± 1	(1.92±0.32)·10^{-10}	(1.32±0.10)·10^{-10}	(2.95±0.41)·10^{-9}	(5.35±0.42)·10^{-10}	This work
80 ± 1	(5.78±0.91)·10^{-10}	(4.68±0.33)·10^{-10}	(2.26±0.35)·10^{-9}	(1.03±0.11)·10^{-9}	This work
Transverse R-GFRP					
20 ± 1	(2.97±0.42)·10^{-10}	(3.97±0.28)·10^{-11}	(1.35±0.19)·10^{-9}	(2.12±0.17)·10^{-10}	This work
40 ± 1	(3.46±0.48)·10^{-10}	(1.41±0.12)·10^{-10}	(1.52±0.21)·10^{-9}	(3.52±0.31)·10^{-10}	This work
60 ± 1	(7.71±0.92)·10^{-10}	(2.40±0.19)·10^{-10}	(5.66±0.79)·10^{-9}	(5.87±0.41)·10^{-10}	This work
80 ± 1	(1.10±0.22)·10^{-9}	(8.02±0.56)·10^{-10}	(3.15±0.42)·10^{-9}	(1.70±0.12)·10^{-9}	This work

The Arrhenius approach was used to obtain steady-state Si's and glass dissolution's activation energy. The activation energy was obtained through graphing at constant pH and σ (zero stress conditions in this study), similarly as was done in previous studies, Equation 21 [9,16]:

$$ln\, K_0 = -\frac{E_A}{R}\frac{1}{T} + ln\, A \tag{21}$$

The graphing approach is shown in Figure 9. Obtained apparent activation energy E_A of Si dissolution is 38.44 and 44.89 kJ/mol (using $K^{II}_{0_{Si}}$ values) for hoop and transverse R-GFRPs, respectively, whereas for unembedded fibers it is 53.46 kJ/mol [16]. The pre-

Preprints (www.preprints.org) | NOT PEER-REVIEWED | Posted: 4 July 2022 doi:10.20944/preprints202207.0027.v1

exponential factor A for Si dissolution is $6.82 \cdot 10^{-1}$ g/(m²·s), the same for both configurations.

Obtained activation energy E_A of total glass dissolution is 24.85 and 31.90 kJ/mol (using $K_{0_{total}}^{II}$ values), for hoop and transverse R-GFRPs, respectively. The pre-exponential factor for glass dissolution A is $1.67 \cdot 10^{-3}$ g/(m²·s) for all configurations. For the non-encapsulated R-GF, the activation energy E_A of total glass dissolution was 34.84 kJ/mol, values reported in [16].

Obtained values are consistent with values reported in the literature for R-GFs [16], but are lower. This effect is considered apparent, as is due to the fact, that ICP-MS captures only ions that have left the composite plates, whereas there is a significant amount of ions accumulating inside. This issue is discussed in more detail in the Discussion.

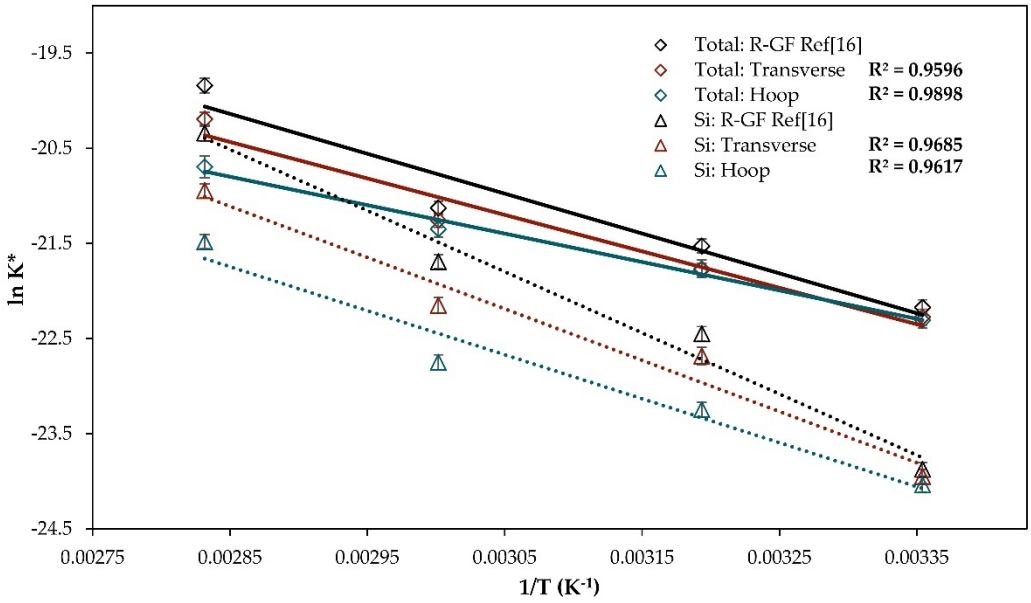

Figure 9. Graphing approach to obtain the pre-exponential factors and activation energies of Si and total glass dissolution for GFRPs at pH 5.65 at 60 °C, compared with unencapsulated R-GF data reported in [16].

Simulating the GFRP dissolution kinetics with the DCZOK model. The ICP-MS data of ion release was used as an input for DCZOK model simulations. The results of the simulations are shown in Figures 10 and 11, where points represent experimental data, and lines represent DCZOK modeled curves using rate constants reported in Tables 2, and 3, respectively. In Figures 10 and 11, the glass mass loss is reported as normalized per the initial surface area of fibers (S_0) as is commonly accepted for surface reaction kinetics [16]. S_0 is calculated based on geometrical considerations and a glass fiber fraction.

Preprints (www.preprints.org) | NOT PEER-REVIEWED | Posted: 4 July 2022 doi:10.20944/preprints202207.0027.v1

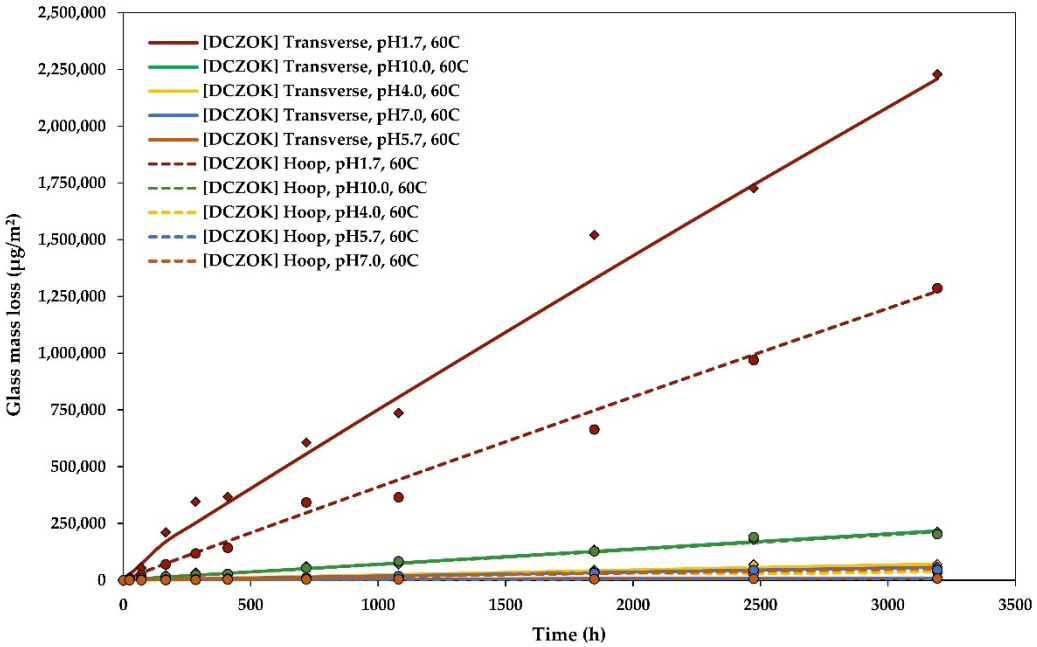

Figure 10. Glass dissolution kinetics at various pH levels: experimental data and modeled DCZOK dissolution curves for GFRP plates.

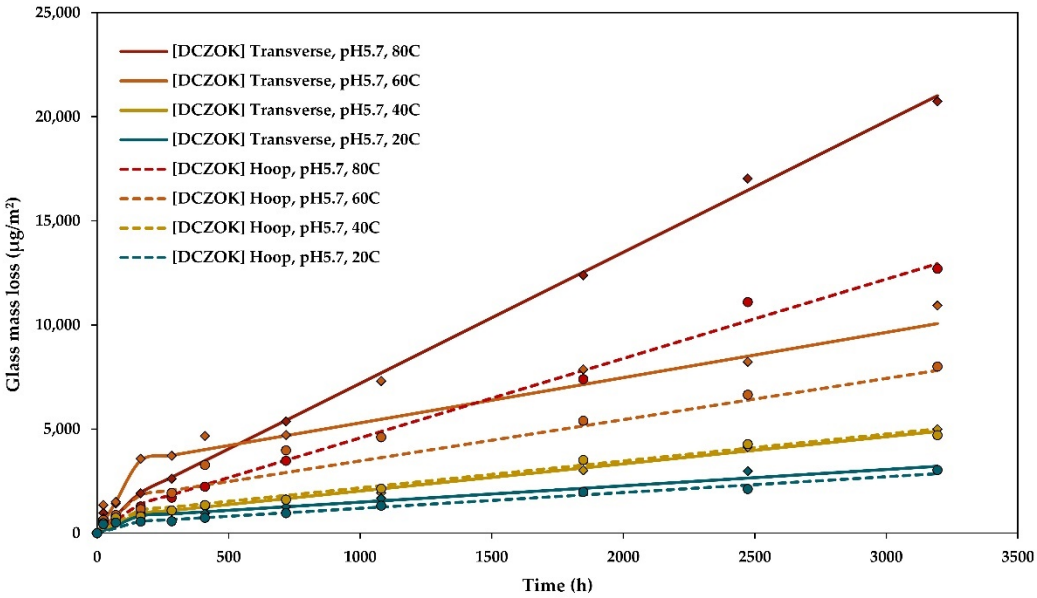

Figure 11. Glass dissolution kinetics at various temperatures: experimental data and modeled DCZOK dissolution curves for GFRP plates.

4. Discussion

Effect of the environment. Like for the R-GFs [16], also for the studied R-GFRPs, the temperature shows a similar Arrhenius-type influence on the kinetics, increasing the rate of dissolution exponentially with increasing temperature. The DCZOK model was able to capture the effect of temperature for R-GFRPs well in both hoop and transverse orientations.

Preprints (www.preprints.org) | NOT PEER-REVIEWED | Posted: 4 July 2022 doi:10.20944/preprints202207.0027.v1

Similar to R-GFs [16], R-GFRPs also showed a hyperbolic dependence on pH. Transverse specimens degraded much quicker at pH 1.7 than their hoop counterparts, and their integrity was destroyed within a week, as seen in Figure 4. Thus, R-GFRPs should not be used in strongly acidic conditions. This finding agrees with an observation in another study, stating that many GFRPs fail catastrophically after a critical time when exposed to acids [17,56]. It is possible to obtain a pH influence on activation energies of dissolution by rearranging Arrhenius equation into the following form, Equation 22:

$$E_A = RT(ln\,A - ln\,K_0) \tag{22}$$

A pH function of the normalized activation energy of dissolution $E_A^{II} = f(pH)$ for R-glass [16] and respective R-GFRPs studied in this work is shown in Figure 12. Normalization is done in respect to activation energy at pH 5.65, which exhibited the lowest activation energy levels. It is commonly accepted to approximate the pH dependency as a polynomial function [16,57].

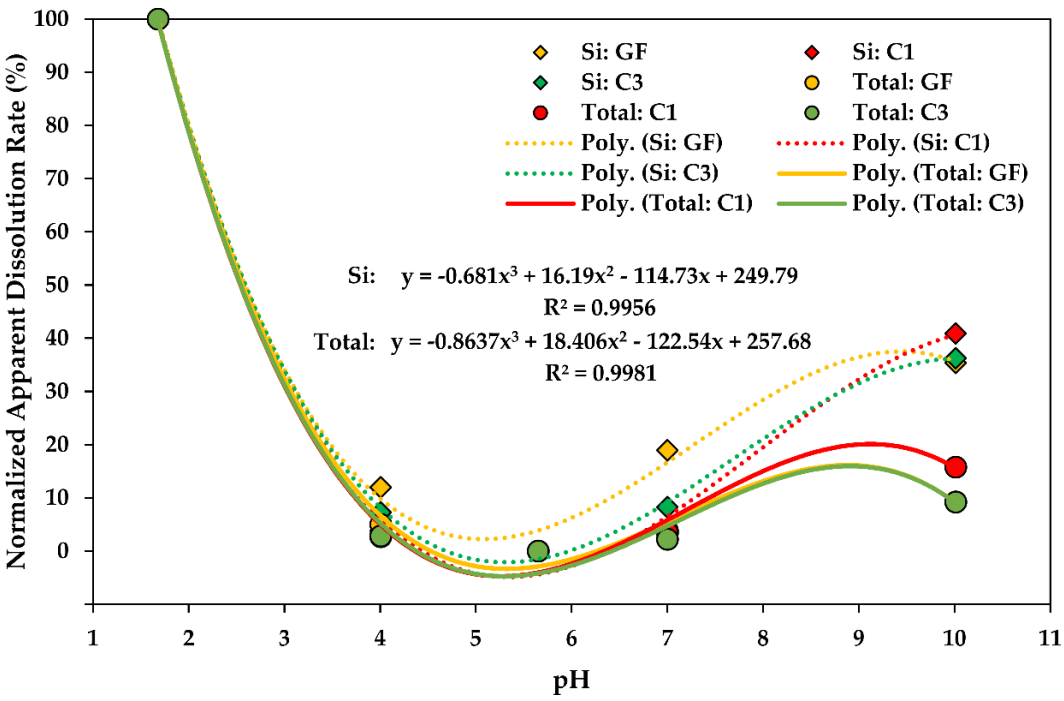

Figure 12. Normalized activation energy of the steady-state glass dissolution as a function of pH for R-GFs [16] and R-GFRPs (legend: C1 and C3 stands for hoop and transverse R-GFRP plates, respectively).

For all cases, the trend of pH influence on the activation energy of dissolution is similar – for both total glass dissolution and Si release. This observation indicates that the total glass dissolution rate constants for various pH levels form a mastercurve for glass fibers and respective GFRPs. Similar is true for Si release. Both glass and Si dissolution rate constant trends are similar with an exception that at high pH levels, i.e., pH 10.0, rates of Si dissolution increase more dramatically than the total glass dissolution rates, indicating a higher contribution of Si to the material loss during the dissolution in basic environments.

Effect of the fiber orientation and embedment. Compared to dissolution of unembedded R-GFs [16], the long-term dissolution of the studied R-GFRPs was slowed down by 36.84% and 65.26% for R-GFRP plates with transverse and hoop fiber orientation, respectively. Slower dissolution from R-GFRPs compared to R-GFs was explained with the

Preprints (www.preprints.org) | NOT PEER-REVIEWED | Posted: 4 July 2022 doi:10.20944/preprints202207.0027.v1

limited water availability and due to silica degradation product accumulation inside the composite.

On the effect of degradation product accumulation and water availability. Unlike the free fibers, for GFRPs, the water availability and degradation product accumulation terms are essential and must be considered when studying kinetics of glass degradation [9]. By using different sample configurations, the authors attempted to decouple water availability and accumulation terms. By using a combination of short interface (sizing) highways (1.5 mm) in transverse R-GFRP plates, where accumulation can be assumed non-present [9,10], and composite hoop R-GFRP plates with comparably long interface highways of 20 mm, it was possible to obtain water availability and accumulation terms separately, similarly as was performed in earlier work [9,10]. The water availability is governed by the water saturation levels of epoxy matrix $C_{H_2O}^{eq}$, being 0.0344 g H_2O/g polymer (3.44 wt%) for the studied polymer [9,50]. Unlike the hoop R-GFRP composite with long interface highways of 20 mm, for the 1.5 mm short-highway transverse R-GFRP plates, it can be assumed that there is no accumulation term [10], so that the time-dependent concentration of silica degradation products $C_{SiO_2}(t)$ is always 0. The whole accumulation term then equals to 1 [10]. The DCZOK model simplifies to Equation 23:

$$\frac{\partial m}{\partial t} = 2n\pi l\left(r_0 K_0 \xi_{sizing} C_{H_2O}^{n_{order}}(t)\left(\frac{C_{SiO_2}^{eq}}{C_{SiO_2}^{eq}}\right)^{m_{order}} - \frac{\left(K_0 \xi_{sizing} C_{H_2O}^{n_{order}}(t)\left(\frac{C_{SiO_2}^{eq}}{C_{SiO_2}^{eq}}\right)^{m_{order}}\right)^2}{\rho_{glass}} t\right) \quad (23)$$

Since the composite plates are thin, the time-dependent water concentration in the polymeric matrix inside the composite $C_{H_2O}(t)$ reaches saturation $C_{H_2O}^{eq}$ very fast. Then, for the steady-state dissolution, the equation simplifies to Equation 24:

$$\frac{\partial m}{\partial t} = 2n\pi l\left(r_0 K_0 \xi_{sizing}\left(C_{H_2O}^{eq}\right)^{n_{order}} - \frac{\left(K_0 \xi_{sizing}\left(C_{H_2O}^{eq}\right)^{n_{order}}\right)^2}{\rho_{glass}} t\right) \quad (24)$$

As can be seen from Equation 24, there are no more unknown time-dependent parameters left in the equation. The only unknown constant is the order of the water availability n_{order}, which then can be obtained from the experimental data using the non-linear regression. Now, for the 20 mm long-highway composite hoop R-GFRP plates, the accumulation of the degradation products cannot be neglected [10], and thus the mass loss Equation 25 can be written as (after water saturation of the polymeric matrix):

$$\frac{\partial m}{\partial t} = 2n\pi l\left(r_0 K_0 \xi_{sizing}\left(C_{H_2O}^{eq}\right)^{n_{order}}\left(\frac{C_{SiO_2}^{eq} - C_{SiO_2}(t)}{C_{SiO_2}^{eq}}\right)^{m_{order}} - \frac{\left(K_0 \xi_{sizing}\left(C_{H_2O}^{eq}\right)^{n_{order}}\left(\frac{C_{SiO_2}^{eq} - C_{SiO_2}(t)}{C_{SiO_2}^{eq}}\right)^{m_{order}}\right)^2}{\rho_{glass}} t\right) \quad (25)$$

As can be seen from Equation 25, there are only two unknown parameters left in the equation, one being the time-dependent concentration of degradation products in the composite $C_{SiO_2}(t)$, and the other one a constant order of the reaction m_{order}. Since m_{order} assumed to be the same for all conditions [10], the $C_{SiO_2}(t)$ and m_{order} are then obtained by fitting the model Equation 25 to the experimental data. Both $C_{SiO_2}(t)$ and

Preprints (www.preprints.org) | NOT PEER-REVIEWED | Posted: 4 July 2022 doi:10.20944/preprints202207.0027.v1

$C_{SiO_2}^{eq}$ are unitless (g SiO_2/g H_2O · g H_2O/g interphase) mass concentrations of silica degradation products per mass of water inside the composite interphase (Equation 26):

$$C_{SiO_2}(t) = \frac{m_{accumulated\ SiO_2}(t)}{m_{interphase} \cdot C_{SiO_2}(t)} \cdot C_{SiO_2}(t) = \frac{m_{accumulated\ SiO_2}(t)}{m_{interphase}} \tag{26}$$

In order to calculate these values, it is necessary to calculate the volume and mass of the interphase $m_{interphase}$, which is assumed constant throughout the process. This can be done from geometrical considerations [9]. The thickness of the interphase ($\delta_{interphase}$) is 0.05 µm, after [9]. The volume is calculated as the difference between the outer (glass and interphase) and the inner (bare glass) cylinders as follows (Equation 27):

$$V_{interphase} = nl\pi\left(r_{sized\ fibres}^2 - r_{bare\ glass}^2\right) \tag{27}$$

The density of the interphase is assumed to be the same as the density of the matrix polymer ($\rho_{interphase} = \rho_{matrix}$), since the interphase consists of about 90% epoxy film former by mass [9,58,59]. The weight of the interphase is roughly 1.01 w% of the sized fibers, which is consistent with another work (0.64 w% of the sized fibers determined via burn-off tests) [9]. It is higher than in the case of burn-of tests, since in reality not the whole fiber surface is uniformly covered with sizing [59]. One can then write Equation 28:

$$m_{interphase} \approx \frac{1.01\ \%}{100\ \%} m_{glass_{initial}} \tag{28}$$

where $m_{glass_{initial}}$ is the initial sized glass fiber mass (g).

The amount of water hosted by the interphase at saturation roughly corresponds to the water saturation levels of the studied epoxy matrix $C_{H_2O}^{eq}$, since about 90% of the interphase is epoxy film former [9,58,59]. The equilibrium concentration of silica degradation products $C_{SiO_2}^{eq}$ is dependent on temperature and can be calculated using relationships provided in another work [9,16], extended for the composite interphase (Equation 29):

$$C_{SiO_2}^{eq} = -\frac{7.31 \cdot 10^{-4}}{T} C_{H_2O}^{eq} + 4.52 \cdot 10^{-6} \cdot C_{H_2O}^{eq} \tag{29}$$

Using Equation 18, the obtained saturation concentration is 2.07, 2.19, 2.33, 2.45 mg SiO_2/kg water, or $C_{SiO_2}^{eq}$ is equal to $7.11 \cdot 10^{-8}$, $7.52 \cdot 10^{-8}$, $8.00 \cdot 10^{-8}$ and $8.43 \cdot 10^{-8}$ g SiO_2/g interphase for 20, 40, 60 and 80 °C, respectively.

Measurements with different sample configurations allowed decoupling water availability and degradation product accumulation terms at various pH and temperatures. Assuming that the effect of sizing ξ_{sizing} is the same at all conditions and equals 0.165 as was reported in another study [10], the order of reaction m_{order} was calculated for various environmental conditions at the steady-state. The order of the reaction of the degradation product accumulation term were calculated for various conditions and are shown in Figure 13. The temperature did not exhibit a strong influence on the order of reaction for water availability.

Preprints (www.preprints.org) | NOT PEER-REVIEWED | Posted: 4 July 2022 doi:10.20944/preprints202207.0027.v1

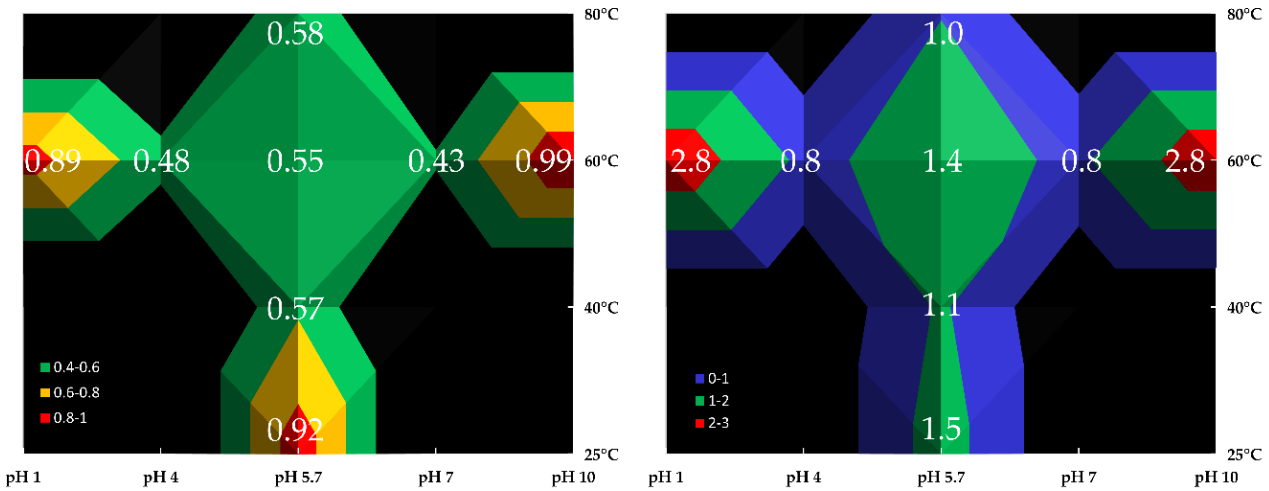

Figure 13. Effect of pH and temperature on the dissolution rate constant (left) and the dissolution activation energy (right). Black areas represent absence of data.

The order of the water availability n_{order} and the order of degradation product accumulation m_{order} were obtained at the steady-state dissolution giving the best fit in regards to the experimental data. They were found to be 0.05 and 1, respectively. These values provided a good fit for all environmental conditions studied. A low value of n_{order} indicates that the water is mostly in free state, i.e., not chemically bound, which is consistent with another work on the same matrix polymer [9]. The obtained m_{order} indicates that the accumulation reaction is linear and bears a close resemblance to the Linear Driving Force (LDF) kinetics [60].

Limitations of the DCZOK approach. The authors think that experimentally and computationally validating the current study with a DCZOK model for seawater conditions (about 1.84 – 12.62 mg SiO_2/kg water; pH of seawater 7.8) would be highly beneficial, especially for the marine and offshore industries, since the real-life structures most often operate in the seawater environment. When GFRPs are used in seawater, glass dissolution occurs slower due to the abundance of silica in the seawater, which is in seawater from the contact with sand and minerals [61,62]. The authors theorize that the model may account for this effect using the degradation product term since the degradation products $C_{SiO_2}(t)$ are already present in the seawater and should slow down the degradation [61,62]. The approach in distilled water is thought to be conservative with regards to seawater, meaning that GFRP structures designed for distilled water conditions should not encounter penalties to their service time in the seawater.

Furthermore, the thickness of the composite is likely to have an influence. It should be more problematic for degradation products to leave the thicker composite. This would mean that the effect of degradation product accumulation should better protect the thicker GFRP structures from glass dissolution. Additional research is needed to test this hypothesis. To use the model for thick structures, the water availability (water concentration) term should be found locally based on the diffusion profiles, i.e., using numerical Finite Element simulations, as described in another work [54]. The local time-dependent water concentrations can be obtained and operated locally in the analytical model by implementing the matrix polymer's water diffusion behavior.

The development of a more precise approach to determine the local degradation product concentration inside the composites would be needed. This would allow predicting local deceleration of the reaction in thick structures and predictions of time in which the degradation products reach the saturation inside the composite if equilibrium can be

Preprints (www.preprints.org) | NOT PEER-REVIEWED | Posted: 4 July 2022 doi:10.20944/preprints202207.0027.v1

achieved. It has been reported that in some cases, after long water exposure, the deterioration of strength of thick GFRP structures seems to stop, i.e., in some ship hulls, while in other cases, the deterioration proceeds, and the saturation is not observed [63]. If the equilibrium occurs, the authors believe this phenomenon may be linked to the accumulation of degradation products inside the structure. If this hypothesis is true, the dissolution of glass inside the composite should stop when $C_{SiO_2}^{eq}$ is reached. According to the estimates using the DCZOK model with the parameters obtained in this work, the time to reach $C_{SiO_2}^{eq}$ for various environmental conditions is shown in Figure 14.

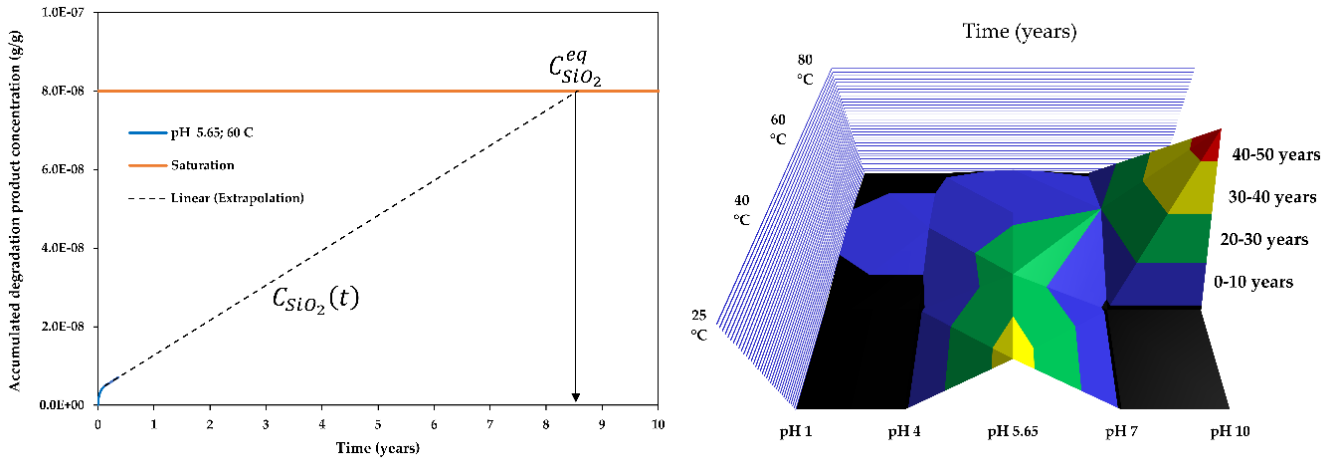

Figure 14. The extrapolation of the time-dependent degradation product concentrations in the interphase was used to estimate the time to saturation (left), and a summary of estimated times to reach the saturation of accumulated silica degradation products inside the composite for various environmental conditions (right). Black areas represen the absence of data.

Estimated times to reach saturation of degradation product inside the composite and the approach to obtain it are shown in Figure 14. The time to reach saturation decreases as the temperature is increased. At pH 5.65, the estimated time to reach saturation at 20, 40, 60, and 80 °C is 24, 15, 8.5, and 1.5 years, respectively. Also, the time to saturate decreases as the environment becomes more acidic. At 60 °C, the estimated time to reach saturation at pH levels of 1.7, 4.0, 5.7, 7.0, and 10.0 are 1.5, 2.5, 8.5, 10, and 36 years, respectively.

Types of GFRPs. R-GFRPs were studied in this work. However, there should be no limitations to applying the DCZOK model to other types of glass fibers and GFRPs. The model should be applicable to other types of glass since SiO2 is the major component in virtually all types of glass [9], but it would be beneficial to validate this model experimentally with other types of glass fibers.

5. Conclusions

The analytical DCZOK model was applied to simulate the long-term glass dissolution experiments of R-GFRPs. The model accounts for the influence of pH, temperature, and the effects of sizing protection, accumulation of degradation products inside the composite, and water availability. The glass dissolution rate constants were obtained and reported for various pH and temperatures.

Temperature exhibited an Arrhenius-type influence on the kinetics of R-GFRP dissolution, increasing the rate of dissolution exponentially with increasing temperature. The activation energy of the steady-state glass dissolution was obtained and reported for composites with various fiber orientations (hoop and transverse). The effect was generally similar to that of the temperature effect on the unembedded R-GF.

Preprints (www.preprints.org) | NOT PEER-REVIEWED | Posted: 4 July 2022 doi:10.20944/preprints202207.0027.v1

The trend of pH influence on the activation energy of dissolution was similar and formed close-to-a-mastercurve for R-GFs and respective R-GFRPs in both hoop and transverse orientations. In comparison with neutral conditions, basic and acidic aqueous environments showed an increase in dissolution rates, affecting the lifetime of glass fiber composites negatively. A higher contribution of Si release to the material loss during the dissolution in basic environments was observed. Composite samples quickly degraded in strongly acidic environment and were destroyed within a week.

Slower dissolution from composites compared to fibers was due to the effects of limited water availability and due to degradation product accumulation inside the composite. The order of the degradation product accumulation term was theorized and compared for various pH and temperatures.

Slower dissolution from composites compared to fibers was due to the effects of limited water availability and due to degradation product accumulation inside the composite. The order of the water availability and the order of the degradation product accumulation term were obtained and were 0.05 and 1, respectively. A low value of n_{order} indicated that the water is mostly in a free state, meaning primarily not chemically bound. The obtained m_{order} indicated that the degradation product accumulation is linear and resembles that of the Linear Driving Force (LDF) kinetics.

Author Contributions: Conceptualization, A.E.K..; methodology, A.E.K., I.Z., I.B., M.K.; software, A.E.K., I.B.; validation, A.E.K.; formal analysis, A.E.K.; investigation, A.E.K.; resources, A.E.K., M.K.; data curation, A.E.K., H.A.A., S.B., J.B., I.Z., I.B., M.K.; writing—original draft preparation, A.E.K., H.A.A., J.B., M.K.; writing—review and editing, A.E.K., H.A.A., S.B., J.B., I.Z., I.B., M.K.; visualization, A.E.K.; supervision, A.E.K.; project administration, A.E.K.; funding acquisition, A.E.K.

Funding: This work was funded by the European Regional Development Fund within the Activity 1.1.1.2 "Post-doctoral Research Aid" of the Specific Aid Objective 1.1.1 of the Operational Programme "Growth and Employment" (Nr.1.1.1.2/VIAA/4/20/606, "Modelling Toolbox for Predicting Long-Term Performance of Structural Polymer Composites under Synergistic Environmental Ageing Conditions").

Institutional Review Board Statement: Not applicable.

Informed Consent Statement: Not applicable.

Data Availability Statement: Not applicable.

Acknowledgments: This work is part of the Postdoctoral Project research funded by the European Regional Development Fund within the Activity 1.1.1.2 "Post-doctoral Research Aid" of the Specific Aid Objective 1.1.1 of the Operational Programme "Growth and Employment" (Nr.1.1.1.2/VIAA/4/20/606). The authors are thankful to Andreas T. Echtermeyer for fruitful discussions, Syverin Lierhagen, and Konstantins Viligurs for help with elemental analyses. Andrey is grateful to Oksana.

Conflicts of Interest: The authors declare no conflict of interest. The funders had no role in the design of the study; in the collection, analyses, or interpretation of data; in the writing of the manuscript, or in the decision to publish the results.

References

1. Krauklis, A.E.; Karl, C.W.; Gagani, A.I.; Jørgensen, J.K. Composite Material Recycling Technology—State-of-the-Art and Sustainable Development for the 2020s. *J. Compos. Sci.* **2021**, 5, 28. doi:10.3390/jcs5010028
2. WindEurope – Cefic – EuCIA. Accelerating Wind Turbine Blade Circularity. White Paper, May 2020.Available online: https://windeurope.org/wp-content/uploads/files/about-wind/reports/WindEurope-Accelerating-wind-turbine-blade-circularity.pdf (accessed on 11 November 2020).
3. Van der Woude, J. (EuCIA) Recycling, Status and Developments in Europe. In Proceedings of the International Glass Fiber Symposium, Aachen, Germany, 29–30 October 2018.
4. Tournié, A.; Ricciardi, P.; Colomban, P. Glass Corrosion Mechanisms: A Multiscale Analysis. *Solid State Ionics* **2008**, 179(38), 2142-2154, doi:10.1016/j.ssi.2008.07.019

Preprints (www.preprints.org) | NOT PEER-REVIEWED | Posted: 4 July 2022 doi:10.20944/preprints202207.0027.v1

5. Bledzki, A.; Spaude, R.; Ehrenstein, G.W. Corrosion Phenomena in Glass Fibres and Glass Fibre Reinforced Thermosetting Resins. *Compos. Sci. Technol.* **1985**, 23(4), 263-285, doi:10.1016/0266-3538(85)90040-5
6. Iler, R.K. *The Chemistry of Silica: Solubility, Polymerization, Colloid and Surface Properties and Biochemistry of Silica*; Wiley: New York, USA, 1979; pp. 896, ISBN:978-0-471-02404-0
7. Wierderhorn, S.M.; Bolz, L.H. Stress corrosion and static fatigue of glass. *J. Am. Ceram. Soc.* **1970**, 53(10), 543-548, doi:10.1111/j.1151-2916.1970.tb15962.x
8. Krauklis, A.E. Modular Paradigm for Composites: Modeling Hydrothermal Degradation of Glass Fibers. *Fibers* **2021**, *9*, 83. https://doi.org/10.3390/fib9120083
9. Krauklis, A.E. Environmental Aging of Constituent Materials in Fiber-Reinforced Polymer Composites. Ph.D. Thesis, NTNU, Trondheim, Norway, 2019; p. 203, ISBN 978-82-326-4027-0
10. Krauklis, A.E.; Echtermeyer, A.T. Dissolving Cylinder Zero-Order Kinetic Model for Predicting Hygrothermal Aging of Glass Fiber Bundles and Fiber-Reinforced Composites. In Proceedings of the 4th International Glass Fiber Symposium, Aachen, Germany, October 2018; Gries, T., Pico, D., Lüking, A., Becker, T., Eds.; pp. 66–72, ISBN 978-3-95886-249-4
11. Echtermeyer, A.T.; Krauklis, A.E.; Gagani, A.I.; Sæter, E. Zero Stress Aging of Glass and Carbon Fibers in Water and Oil—Strength Reduction Explained by Dissolution Kinetics. *Fibers* **2019**, *7*, 107. https://doi.org/10.3390/fib7120107
12. Echtermeyer, A.T.; Gagani, A.I.; Krauklis, A.E.; Mazan, T. Multiscale Modelling of Environmental Degradation—First Steps. In Durability of Composites in a Marine Environment 2. Solid Mechanics and Its Applications; Davies, P., Rajapakse, Y.D.S., Eds.; Springer: Cham, Switzerland, 2018; Volume 245, pp. 135–149. ISBN 978-3-319-65145-3
13. McGeorge, D.; Echtermeyer, A.T.; Leong, K.H.; Melve, B.; Robinson, M.; Fischer, K.P. Repair of floating offshore units using bonded fibre composite materials. Compos. Part A **2009**, 40, 1364–1380
14. Grabovac, I.; Whittaker, D. Application of bonded composites in the repair of ships structures—A 15-year service experience. Compos. Part A **2009**, 40, 1381–1398
15. Krauklis, A.E.; Karl, C.W.; Rocha, I.B.C.M.; Burlakovs, J.; Ozola-Davidane, R.; Gagani, A.I.; Starkova, O. Modelling of Environmental Ageing of Polymers and Polymer Composites—Modular and Multiscale Methods. *Polymers* **2022**, *14*, 216. https://doi.org/10.3390/polym14010216
16. Krauklis, A.E.; Gagani, A.I.; Vegere, K.; Kalnina, I.; Klavins, M.; Echtermeyer, A.T. Dissolution Kinetics of R-Glass Fibres: Influence of Water Acidity, Temperature, and Stress Corrosion. *Fibers* **2019**, *7*, 22. https://doi.org/10.3390/fib7030022
17. Krauklis, A. The Effect of Strong Acids on Glass Fibre Reinforced Composites; SINTEF Report 102017059-3-12; SINTEF: Oslo, Norway, 2019.
18. Corrosion Resistance of Glass Fibre Materials - A Crucial Property for Reliability and Durability of FRP Structures in Aggressive Environments
19. Kouassi S, Andji J, Bonnet J, Rossignol S (2010). Dissolution of waste glasses in high alkaline solutions. Ceram Silik 54(3):235–240.
20. S. T. Bashir, L. Yang, J. J. Liggat & J. L. Thomason (2017). Kinetics of dissolution of glass fibre in hot alkaline solution Journal of Materials Science volume 53, pages 1710–1722
21. Tatiana Trejos, Shirly Montero & José R. Almirall (2003). Analysis and comparison of glass fragments by laser ablation inductively coupled plasma mass spectrometry (LA-ICP-MS) and ICP-MS. Analytical and Bioanalytical Chemistry volume 376, pages 1255–1264
22. Jo Ann Buscaglia, Elemental analysis of small glass fragments in forensic science, Analytica Chimica Acta, Volume 288, Issues 1–2,1994, Pages 17-24, ISSN 0003-2670, https://doi.org/10.1016/0003-2670(94)85112-3
23. Stoecklein W, Becker S (2001) Proceedings of the 13th Interpol Forensic Science Symposium, October, 2001, Lyon, France
24. Kristian von Wuthenau, Torben Segelke Anita Kuschnereit Markus Fischer (2021). Glass authentication: Laser ablation-inductively coupled plasma mass spectrometry (LA-ICP-MS) for origin discrimination of glass bottles. Talanta. Volume 235, 1, 122686
25. Krauklis, A.E.; Gagani, A.I.; Echtermeyer, A.T. Long-Term Hydrolytic Degradation of the Sizing-Rich Composite Interphase. Coatings **2019**, 9, 263
26. Krauklis, A.E.; Echtermeyer, A.T. Long-Term Dissolution of Glass Fibers in Water Described by Dissolving Cylinder Zero-Order Kinetic Model: Mass Loss and Radius Reduction. Open Chem. **2018**, 16, 1189–1199
27. Walter Eastes, Russell M. Potter, John G. Hadley (2000) ESTIMATING IN VITRO GLASS FIBER DISSOLUTION RATE FROM COMPOSITION, Inhalation Toxicology, 12:4, 269-280, DOI: 10.1080/089583700196149
28. J. Hughes, T. Catterick, G. Southeard (1976). The quantitative analysis of glass by atomic absorption spectroscopy. Forensic Sci., 8, pp. 217-227
29. B. Wagner, A. Nowak, E. Bulska, J. Kunicki-Goldfinger, O. Schalm, K. Janssens (2008). Complementary analysis of historical glass by scanning electron microscopy with energy dispersive X-ray spectroscopy and laser ablation inductively coupled plasma mass spectrometry. Microchimica Acta, 162 (3–4), pp. 415-424
30. R. Coleman, N. Weston (1968). A case concerning neutron activation analysis of glass J. Forensic Sci. Soc., 8 (1), pp. 32-33
31. J.S.U.Schell, M.Renggli G.H.van Lenthe R.Müller P.Ermanni (2006). Micro-computed tomography determination of glass fibre reinforced polymer meso-structure. Composites Science and Technology. Volume 66, Issue 13, Pages 2016-2022
32. J.P. Dunkers, F.R. Phelan, D.P. Sanders, M.J. Everett, W.H. Green, D.L. Hunston (2001). The application of optical coherence tomography to problems in polymer matrix composites. Opt Laser Eng, 35 , pp. 135-147

Preprints (www.preprints.org) | NOT PEER-REVIEWED | Posted: 4 July 2022 doi:10.20944/preprints202207.0027.v1

33. Michalske, T.A.; Freiman, S.W. A Molecular Mechanism for Stress Corrosion in Vitreous Silica. J. Am. Ceram. Soc. **1983**, 66, 284–288
34. Delage, F.; Ghaleb, D.; Dussossoy, J.L.; Chevallier, O.; Vernaz, E. A mechanistic model for understanding nuclear waste glass dissolution. *J. Nucl. Mater.* **1992**, 190, 191-197, doi:10.1016/0022-3115(92)90086-Z
35. Geisler-Wierwille, T.; Nagel, T.J.; Kilburn, M.R.; Janssen, A.; Icenhower, J.; Fonseca, R.O.C.; Grange, M.L.; Nemchin, A.A. The Mechanism of Borosilicate Glass Corrosion Revisited. *Geochim. Cosmochim. Acta* **2015**, 158, 112-129, doi:10.1016/j.gca.2015.02.039
36. Icenhower, J.; Steefel, C.I. Dissolution Rate of Borosilicate Glass SON68: A Method of Quantification Based upon Interferometry and Implications for Experimental and Natural Weathering Rates of Glass. *Geochim. Cosmochim. Acta* **2015**, 157, 147-163, doi:10.1016/j.gca.2015.02.037
37. Ma, T.; Jivkov, A.P.; Li, W.; Liang, W.; Wang, Y.; Xu, H.; Han, X. A mechanistic model for long-term nuclear waste glass dissolution integrating chemical affinity and interfacial diffusion barrier. *J. Nucl. Mater.* **2017**, 486, 70-85, doi:10.1016/j.jnucmat.2017.01.001
38. Geisler, T.; Dohmen, L.; Lenting, C.; Fritzsche, M.B.K. Real-time in situ observations of reaction and transport phenomena during silicate glass corrosion by fluid-cell Raman spectroscopy. *Nature Materials* **2019**, 18, 342-348, doi:10.1038/s41563-019-0293-8
39. Grambow, B.; Müller, R. First-order dissolution rate law and the role of surface layers in glass performance assessment. *J. Nucl. Mater.* **2001**, 298(1-2), 112-124. doi:10.1016/S0022-3115(01)00619-5
40. Hunter, F.M.I.; Hoch, A.R.; Heath, T.G.; Baston, G.M.N. *Report RWM005105, AMEC/103498/02 Issue 2: Review of Glass Dissolution Models and Application to UK Glasses*; AMEC: Didcot, Oxfordshire, UK, 2015
41. Grambow B. A General Rate Equation for Nuclear Waste Glass Corrosion. *Mat. Res. Soc. Symp. Proc.* **1985**, 44, 15-27
42. White, J.R. Polymer Ageing: Physics, Chemistry or Engineering? Time to Reflect. *C.R. Chim.* **2006**, 9, 1396–1408, doi:10.1016/J.CRCI.2006.07.008
43. Badia, J.D.; Gil-Castell, O.; Ribes-Greus, A. Long-Term Properties and End-of-Life of Polymers from Renewable Resources. *Polym. Degrad. Stab.* **2017**, 137, 35–57, doi:10.1016/J.POLYMDEGRADSTAB.2017.01.002
44. Putnis, C.V.; Ruiz-Agudo, E. The mineral–water interface: Where minerals react with the environment. Elements **2013**, 9, 177–182
45. Starkova, O.; Gagani, A.I.; Karl, C.W.; Rocha, I.B.C.M.; Burlakovs, J.; Krauklis, A.E. Modelling of Environmental Ageing of Polymers and Polymer Composites—Durability Prediction Methods. *Polymers* **2022**, *14*, 907. https://doi.org/10.3390/polym14050907
46. Wang, M.; Xu, X.; Ji, J.; Yang, Y.; Shen, J.; Ye, M. The hygrothermal aging process and mechanism of the novolac epoxy resin. Compos. Part B **2016**, 107, 1–8
47. Halpin, J.C. Effects of Environmental Factors on Composite Materials; Technical Report AFML-TR-67–423; Air Force Materials Laboratory: Dayton, OH, USA, 1969
48. International Standard ISO 2078:1993 (revised in 2014), Textile Glass—Yarns—Designation. 2014. Available online: https://www.iso.org/standard/6865.html (accessed on 11 February 2019)
49. 3B Fibreglass technical data sheet. HiPer-tex W2020 rovings, Belgium. 2012. Available online: https://www.3b-fibreglass.com/ (accessed on 24 July 2018)
50. Krauklis, A.E.; Gagani, A.I.; Echtermeyer, A.T. Near-Infrared Spectroscopic Method for Monitoring Water Content in Epoxy Resins and Fiber-Reinforced Composites. *Materials* **2018**, *11(4)*, 586-599, doi:10.3390/ma11040586
51. ASTM D3171/D3171-15 Standard Test Methods for Constituent Content of Composite Materials; ASTM International: West Conshohocken, PA, USA, 2015
52. Gagani, A.I.; Fan, Y.; Muliana, A.H.; Echtermeyer, A.T. Micromechanical modeling of anisotropic water diffusion in glass fiber epoxy reinforced composites. J. Compos. Mater. **2017**, 52, 2321–2335
53. Crank J. *The mathematics of diffusion*. Oxford university press, 1956
54. Gagani, Abedin & Krauklis, Andrey & Echtermeyer, Andreas. (2018). Orthotropic fluid diffusion in composite marine structures. Experimental procedure, analytical and numerical modelling of plates, rods and pipes. Composites Part A Applied Science and Manufacturing. 10.1016/j.compositesa.2018.09.026
55. Krauklis, A.E.; Gagani, A.I.; Echtermeyer, A.T. Prediction of Orthotropic Hygroscopic Swelling of Fiber-Reinforced Composites from Isotropic Swelling of Matrix Polymer. *J. Compos. Sci.* **2019**, *3*, 10. https://doi.org/10.3390/jcs3010010.
56. Agarwal, B.D.; Broutman, L.J. *Analysis and Performance of Fibre Composites*, 2nd ed.; John Wiley and Sons, Inc.: Hoboken, USA, 1990; pp. 339-359, ISBN: 978-0-471-51152-6
57. Krauklis, A.E.; Ozola, R.; Burlakovs, J.; Rugele, K.; Kirillov, K.; Trubaca-Boginska, A.; Rubenis, K.; Stepanova, V.; Klavins, M. FeOOH and $Mn_8O_{10}Cl_3$ Modified Zeolites for As(V) Removal in Aqueous Medium. J. Chem. Technol. Biotechnol. **2017**, 92, 1948–1960
58. Krauklis, A.E.; Echtermeyer, A.T. Mechanism of Yellowing: Carbonyl Formation during Hygrothermal Aging in a Common Amine Epoxy. *Polymers* **2018**, 10(9), 1017-1031, DOI: 10.3390/polym10091017
59. Thomason, J.L. *Glass Fiber Sizings: A Review of the Scientific Literature*; J.L.Thomason: Middletown, DE, USA, 2012; pp. 127, ISBN: 978-0-9573814-1-4

Preprints (www.preprints.org) | NOT PEER-REVIEWED | Posted: 4 July 2022 doi:10.20944/preprints202207.0027.v1

60. Kim, D.H. Linear Driving Force Formulas for Diffusion and Reaction in Porous Catalysts. *AlChE J.* **1989**, 35(2), 343-346. DOI: 10.1002/aic.690350225
61. Von Damm, K.L.; Edmond, J.M.; Grant, B.; Measures, C.I.; Walden, B.; Weiss, R.F. Chemistry of submarine hydrothermal solutions at 21°N, East Pacific Rise. *Geochim. Cosmochim. Acta* **1985**, 49, 2197-2220. DOI: 10.1016/0016-7037(85)90222-4.
62. Holland, H.D. *The chemistry of the atmosphere and oceans*; Wiley: New York, USA, 1978; pp. 351, ISBN: 978-0471035091.
63. Chakraverty, A.P.; Mohanty, U.K.; Mishra, S.C.; Satapathy, A. Sea Water Ageing of GFRP Composites and the Dissolved Salts. *IOP Conf. Ser.: Mater. Sci. Eng*. **2015**, 75, 12-29. DOI: 10.1088/1757-899X/75/1/012029